Active Balancing of Lithium-ion Cells for Maximum Power Discharging

By

David Capano

A Thesis Submitted in Partial Fulfillment
of the Requirements for the Degree of

Master of Applied Science

in the

Faculty of Engineering and Applied Science
Department of Electrical, Computer, and Software Engineering
University of Ontario Institute of Technology

July, 2018

Abstract

Active Balancing of Lithium-ion Cells for Maximum Power Discharging

By David Capano

The future of Electric Vehicle's (EV) depends on the adoption of the technology. Currently the limiting factor for EV adoption is mainly the initial cost, the driving range, charging capability, and the battery life. The battery of any EV plays a part into all the major limiting factors in the adoption of EV's in the automotive industry. The most common type of battery found in EVs is the Lithium-ion (Li-ion) battery. It is an adequate battery technology, but it is still fairly heavy, expensive to produce, does not charge very quickly, has a relatively short life-span, and is not the most energy and power dense battery chemistry. A few of these characteristics can be remedied by the Battery Management System (BMS) which is required in any Lithium chemistry battery system to keep the cells in the optimal operating conditions. The BMS in standard EV batteries employ series cell balancing only while charging. The discharge balancing technique can be used to increase useable capacity from an EV battery because at the end of a cycle the stronger cells have some remaining capacity which can be discharged into weaker cells.

This work explores the difference in useable capacity with active cell balancing vs. passive balancing for both new and aged cells near End of Life (EOL). The cell equalizer is designed, simulated, and tested in this work with a simple controller which is effective in demonstrating the increase in useable capacity that can be achieved from active discharge balancing while the Li-ion cells are discharged at or near their maximum power capability. In this work the proposed discharge balancing technique has been researched, simulated, and implemented in hardware testing.

Acknowledgments

I would like to express my gratitude and thankfulness to my supervisor, Dr. Sheldon S Williamson for his guidance and support throughout the course of this work. Without his encouragement to pursue graduate studies I would not find myself where I am today, and I am very thankful for that. Due to his continued pursuit for novel and relevant research work, I have been able to learn from him and be a part of the astounding STEER group that he has created at UOIT. I would like to thank him for the knowledge, perseverance, and leadership qualities, that he has taught me in the time that I have been part of the team.

I would also like to thank my peers and friends in the STEER group and at UOIT. To Dr. Lalit Patnaik who is a Post-Doctoral Fellow in the STEER group and an incredible mentor. I am thankful for his guidance in assisting me with support and knowledge to help me complete my work. For my peers and friends at UOIT I would like to thank them for helping me to make my time with the team, one that I will never forget and will always cherish.

To my family who gave me all the love and support throughout my life. Without their support and nurturing love, I would not be the person I am. I dedicate this dissertation to my family for their commitment to raising me and giving me all their love.

Dedicated to My Family.

Contents

List of Figures

List of Tables

List of Abbreviations

ANN	Artificial Neural Network
BMS	Battery Management System
CC	Constant Current
CV	Constant Voltage
DOD	Depth of Discharge
ECU	Electronics Control Unit
EKF	Extended Kalman Filter
EMF	Electro-Motive Force
EOL	End of Life
EV	Electric Vehicle
I2C	Inter Integrated Circuit Bus
ICE	Internal Combustion Engine
Li-ion	Lithium-ion
MBMS	Module Battery Management System
MOSFET	Metal-Oxide-Semiconductor Field-Effect Transistor
NiCd	Nickel-Cadmium
NiMH	Nickel Metal Hydride
OCV	Open Circuit Voltage
PBMS	Pack Battery Management System
PCB	Printed Circuit Board
QRZCS	Quasi-Resonant Zero Current Switching
SEI	Solid-Electrolyte Interphase
SOC	State of Charge
SOH	State of Health
SPI	Serial Peripheral Interface Bus

List of Symbols

Ah	Ampere-hour	Ah
V	Voltage	V
I	Current	A
C	Capacitance	F
L	Inductance	H
R	Resistance	Ω
f	Frequency	Hz
D	Duty Cycle	%

Chapter 1

Introduction

1.1 The Historic and Futuristic Perspective

In the modern automotive era a massive shift in the drivetrain technology is right around the corner. The shift involves a complete change from Internal Combustion Engines (ICE) to an electric drivetrain. The idea of using electricity is not new. In the mid 1800's electric carriages were built and used to transport people. Ultimately, in the 1920's the advancements made on ICE were pushing the boundaries on speed, driving range, vehicle affordability, and convenience of the use of vehicles [1]. This along with the advancements made by Henry Ford in the way vehicles could be mass manufactured using assembly lines, pushed electric vehicles out of the minds of most companies and inventors. It started a new age based around the harnessing of energy from oil resources. The focus solely on advancements on internal combustion engines was continued until the mid 1960's when the effects of mass combustion of different fuels finally appeared. Smog became a big issue because of incomplete combustion from a lack of catalytic converters which are now a mandatory requirement of ICE vehicles. The realization that burning fuel is not clean nor is it beneficial to the environment brought the initial recognition of how electric vehicles could be utilized to reduce pollution and green house gas emissions.

Greenhouse gases and pollution as a result of burning fuel in combustion engines was not enough to switch the mentality of society to stop burning fuel and research electric vehicles further. The economic aspect to using ICE vehicles instead of EV's is the main driving factor that would ultimately begin to turn the tides on ICE vehicles. Another factor pushing people away from ICE vehicles is the ever-increasing price of oil. This is due to a high demand for the finite resource and

companies and comities which are able to manipulate prices to keep them high. This now brings the economic benefits of EV's closer to what the ICE vehicles currently can offer and as time goes on the future of the EV proves to be very bright.

1.2 Motivation

The change from ICE vehicles to EV's is a large endeavour that will require lots of investment, advancements, and ultimately time. We are currently in an age where the technology currently available is enough to begin to drive mass manufacturing of EV's. Another limiting factor on the adoption of EV's is something psychological with the mass of the population and this is the way that society views electric vehicles. Currently most populations do not entirely understand how electric vehicles work or have misconceptions of the battery in EV's [2]. Over time society will adapt and certain aspects of an ICE vehicle can be related to EV's. The comparison that can be made to bridge the understanding of ICE drivetrains to EV drivetrains is that the gas tank is changing to a battery, the fuel delivery system is being replaced by a motor controller, and the core of the engine now becomes an electric motor. This shift that is coming is due to great advancements in battery technology, power electronics, and motor design, which eventually society will completely understand. Another benefit of electric drivetrains over ICE is there is no need for a multi-speed transmission, therefore meaning a more efficient overall system. The electric drivetrains are slowly becoming cheaper, more durable, more compact, and improving the range of the vehicle.

With all these benefits of an electric drivetrain that can be advertised we must ask, why are electric cars not being adopted faster? The answer is that the vehicles are initially expensive, have a limited range, long charge times, and concerns of the battery lifespan. This can be seen by Figure 1.1, [3].

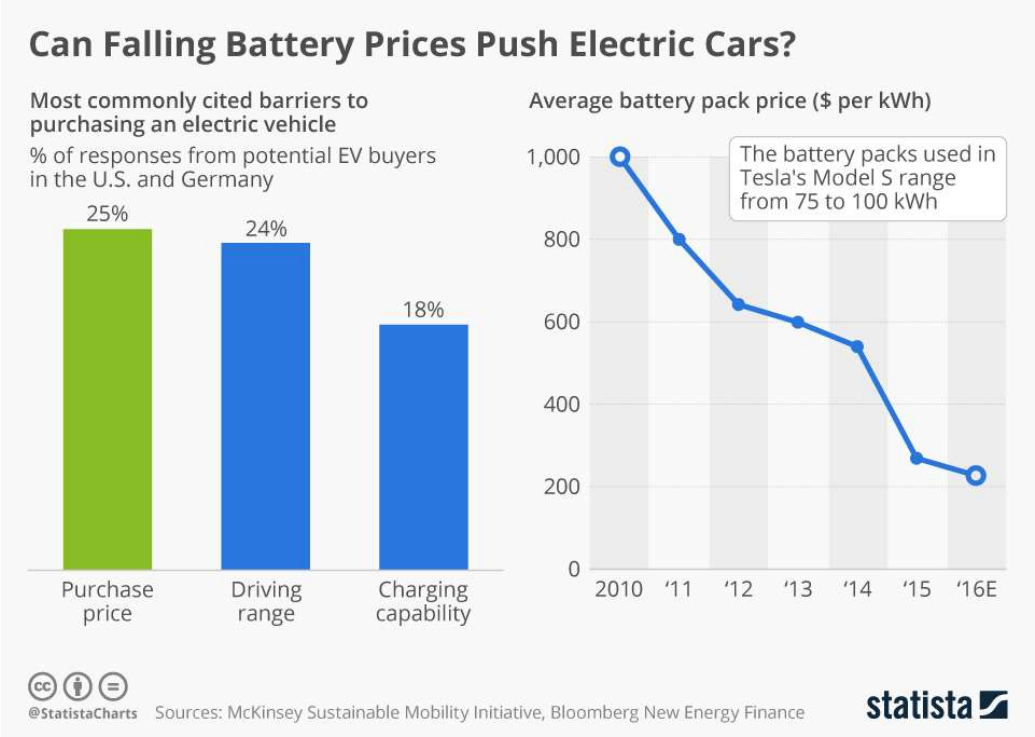

Figure 1.1: Statistics on EV buyer concerns

All of this relates to one area in the EV that is limiting the adoption of electric drivetrains and that is the battery. The battery is the main limiting factor on the driving range, charging speed, and power capabilities [4],[5]. The battery also contributes most of the electric vehicle drivetrain weight, cost, and is the factor by which the lifetime of the drivetrain is evaluated [6],[7]. Battery technology in the last 20 years has greatly improved over the batteries used in the first modern era EV's. The history of the rechargeable battery begins the lead-acid battery which uses lead electrodes and a sulphuric-acid based electrolyte. These batteries were the first rechargeable battery technology to be used in EV's. Their main drawback was their small capacity among other drawbacks such as heavy weight, slow charge time, and large size. The next main battery technology to come into the market was the Nickel Cadmium (NiCd) battery which is an alkaline type battery. This battery chemistry was more energy dense than lead-acid, but it is more expensive and more toxic due to the Cadmium element. The last alkaline battery chemistry to be used was the Nickel Metal Hydride (NiMH) battery. The NiMH battery chemistry is an improvement on the NiCd battery chemistry. The advantages to the NiMH over the NiCd chemistry are improved lifespan, cheaper production costs, and are not as hazardous because of the replacement of the

Cadmium. One of the major drawbacks that were part of the demise to the alkaline batteries was the effect of “battery memory” [8]. This was a major drawback for batteries that did not get full discharge cycles. If a battery was repeatedly cycled and did not undergo fully discharge cycles they would tend to lose their full capacity, and this was coined as the battery memory effect.

The most recent advancements in battery technology have all been around the lithium element. Lithium is the metal element with an extremely high specific capacity of 3860 mAh/g, making it a great element to use as an energy storage component [9]. Like all batteries the lithium battery contains an anode, electrolyte, and cathode. The cathode is where many advancements and changes have been made to the lithium chemistry over the past 20 years. With the lithium type of battery there are many variations of the other materials that make them up. Most chemistries would include Lithium-Polymer, Lithium-Iron Phosphate, and many more which have different cathode elements to give them different characteristics. For the most-part the characteristics for lithium batteries include fast charge times, high energy and power densities, low weight, and longer life cycles [10]. Lithium-ion is the current battery technology which is the most common. They are made up from a cathode that are most commonly made up from metals, or mixes of these metals, which are combined with Lithium and oxidised. Some metals include Manganese, Cobalt, Nickel, Titanium, and Aluminum. They typically have an anode that is made from graphite, sometimes with additives to improve certain characteristics, and the electrolyte made from a lithium salt.

Along with the battery cells themselves there are certain boundaries that must be sustained to get the most life from the cells. Boundaries such as temperature limits, charging rate limits, discharge current limits, and maximum / minimum cell voltage limits. These are all monitored and controlled by a system that must be built into a complete battery pack. This system is called the Battery Management System (BMS) and is considered to be the brain of the battery pack itself.

1.3 EV Battery Systems

The EV battery is a complex component of the electric drivetrain with multiple properties that need to be monitored and controlled to optimize the life of the battery cells and keep cost low. The BMS is the brain behind the control and monitoring of the cells as they charge and discharge

during the life of the EV. It has critical aspects in the control of the voltage boundaries, current limitations, thermal control of the cells, and determining the maximum power capabilities as the State of Charge (SOC) changes. In Figure 1.2 [11], the hierarchy of the EV battery can be seen.

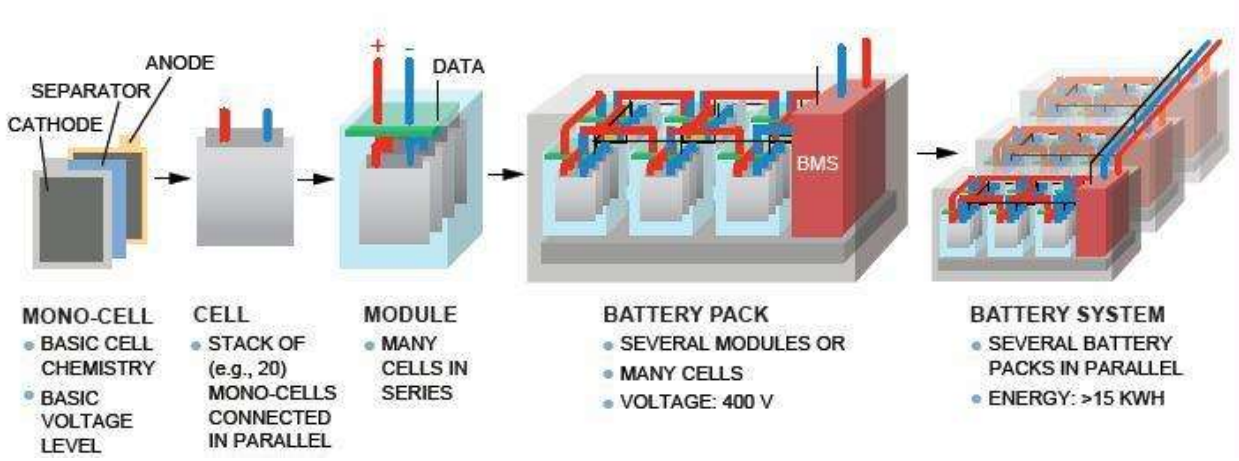

Figure 1.2: EV Battery Architecture

The building blocks of any EV battery are the battery cells which are single cells and in this case Lithium-ion cells with a nominal voltage of 3.7 V. The cells are arranged into series or parallel strings to get the desired nominal voltage and capacity. The assembly of series cells increases the nominal voltage of a module and keep the same capacity, which is rated in Ampere-hours (Ah). The assembly of parallel cells will keep the same nominal voltage but increase the capacity in Ah. In a module there are usually one or more temperature sensors as well as voltage sense leads for the BMS to connect to. Sometimes the module itself may have a current sensor so the individual current of each module can be monitored but typically the current is measured at the terminals of the whole battery pack. The battery pack is then assembled with many modules, once again, in series or parallel depending on the design specifications. At the battery pack level all the cooling channels, are connected to the modules, these cooling channels can be air or liquid but typically a liquid cooling system is chosen as it allows for more control of the cell temperatures as well as a more compact battery pack design [12]. The battery pack in an EV can be a single large pack in one container or a multitude of battery packs spread around the vehicle.

The BMS which is in the module and battery pack is the main governing system for monitoring, maintaining, and controlling the battery. The main responsibilities of the BMS are to

monitor the cell temperature, series cell voltages, module or pack current, estimate SOC, and perform series cell balancing. The BMS structure is typically made of two parts and that is the Pack BMS (PBMS) and the Module BMS (MBMS) which are in each module. The PBMS is the main computer and it communicates with the MBMS to gather and process data. This data can be communicated to the Electronic Control Unit (ECU) and then be transmitted to other vehicle equipment that require battery data as seen in Figure 1.3. The BMS is structured this was to reduce the system complexity and amount of sense wires in a battery pack. This system also reduces the complexity of the series cell balancing in a module.

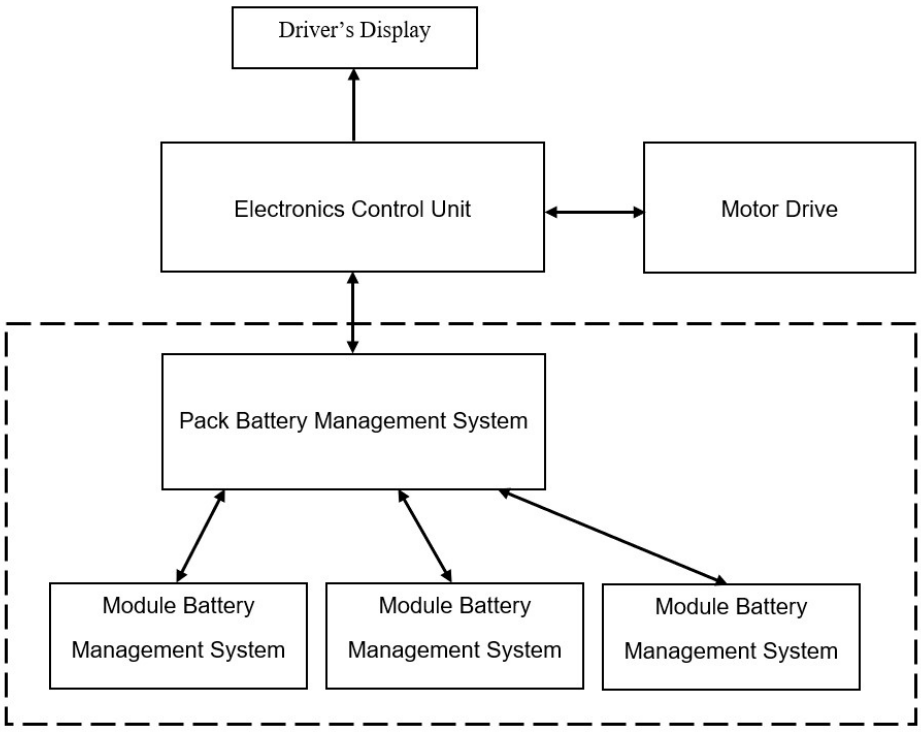

Figure 1.3: Basic EV Data Distribution Flow

1.4 Literature Review and Challenges

The research on maximizing the efficiency and useable capacity of a battery pack has been a large area of research. Along with many billions of dollars spent on research into advanced battery technologies, a lot of money has been put into maximizing the capacity and life of current battery technology. One area that has been explored external of the battery cell itself is the cell

balancing in the MBMS. Cell balancing is required in EV applications due to the impurities during mass manufacturing of Lithium-ion cells, differential aging to due heat gradient in a battery pack, and the differential aging caused by other external factors such as bus bar connection imperfections or high-ripple BMS active cell balancing. Cell balancing is used to protect the weakest series cell from going beyond the voltage boundaries during charging. A new possibility to increase the range for batteries with different series cell capacities, due to aging or other factors, is to also balance the cells while discharging. There are two standard categories for cell balancing and these are passive and active cell balancing [13].

The technique of passive balancing uses a system that has resistors discharge a cell during the charge cycle to then even its voltage with the other cells in a module. This allows all the cells to come up to the full charge voltage evenly and prevent over-voltage of the weaker cell. Active balancing incorporates a means of transferring energy from one cell to another. During the charge cycle the weaker cell reaches full charge faster so the weaker cell transfers energy to the stronger cell. During discharge the weaker cell will reach the end voltage faster and thus the stronger cell will have to transfer energy to the weaker cell. There are many cell equalizers that are capable of doing this such as switched energy storage devices [14]-[18], DC-DC converter based topologies [19],[20], and transformer-based topologies [21],[22].

Overall, there are many different types of cell balancing topologies for passive and active balancing which have their own advantages and disadvantages. The topology used for cell balancing and the control of that topology is a commonly researched topic.

1.5 Scope of Thesis

Throughout all the studies on cell balancing techniques, the focus has been on the emphasis of faster balancing during charging, more efficient cell balancers, or improved control. The scope of this thesis is on cell balancing during cell discharge which can increase the useable capacity of a battery pack that utilizes an industry standard BMS which considers a battery pack to be at 0% SOC when the first cell has reached the set cut-off voltage.

The objective of this thesis is to use an active balancing technique to harness the unused capacity of a strong cell in a series string to assist a weaker cell. This unused capacity will be used to reduce the load on the weaker cell and thus reduce the voltage sag across it therefore balancing the stronger and weaker cell voltages. This in turn will increase the range of a Lithium-ion battery pack that utilizes an industry standard BMS which has a set cut-off voltage at which the battery pack is considered 0%. The thesis has been divided into the following chapters as outlined below.

- Chapter 1: Introduction
- Chapter 2: All aspects and parts of the BMS are studied with the characteristics of Lithium-ion batteries related to the operations of the BMS.
- Chapter 3: The discharge balancing perspective to the BMS is investigated and certain functions are defined in order to accomplish this task. Along with the design, control, and simulations of an active balancer capable of discharge balancing.
- Chapter 4: The discharge balancing technique is validated through hardware experimental results.
- Chapter 5: Concludes the findings and contributions of this thesis. Details for future work are also outlined.

Chapter 2

Cell Balancing Techniques

In a string of series batteries, the voltages of each cell in series may not be the exact same as the others. This is due to chemical differences in the cells electrochemistry of its components. This can occur because of differences in cell temperature over the life of the battery or due to imperfections in the manufacturing process. The two generalized methods of cell balancing are passive cell balancing and active cell balancing. Passive cell balancing takes use of resistors that are connected in parallel with the cell and engaged when one series cell voltage is higher than the others and the voltage must be reduced to balance them. Active balancing uses converters or other power electronic methods of transferring energy from one cell to another to balance the series cell voltages. This chapter explains the characteristics of Lithium-ion cells, SOC estimation, and summarizes the many methods and techniques used for balancing the series cell voltages in a string of cells.

2.1 Lithium-ion Battery Characteristics

The Li-ion battery is a relatively simple electrochemical energy storage device when looking at its components in the most basic way. The cathode, or positive terminal, is typically a metal oxide or combination of oxidised metals which typically are composed of Cobalt, Nickel, Manganese, Aluminum, Titanium, or Iron-Phosphate [23]. These metals are used due to their ability to accept or release ionized lithium atoms which then migrate in the electrolyte and are then deposited in the anode. The basic layout of a Li-ion cell is shown in Figure 2.1.1. The anodes are typically made of a graphite or doped graphite material. The difference between single metal cathodes or mixed cathodes include, specific energy, thermal runaway temperature (safety), cycle life, cost, charge/discharge capabilities, and specific power.

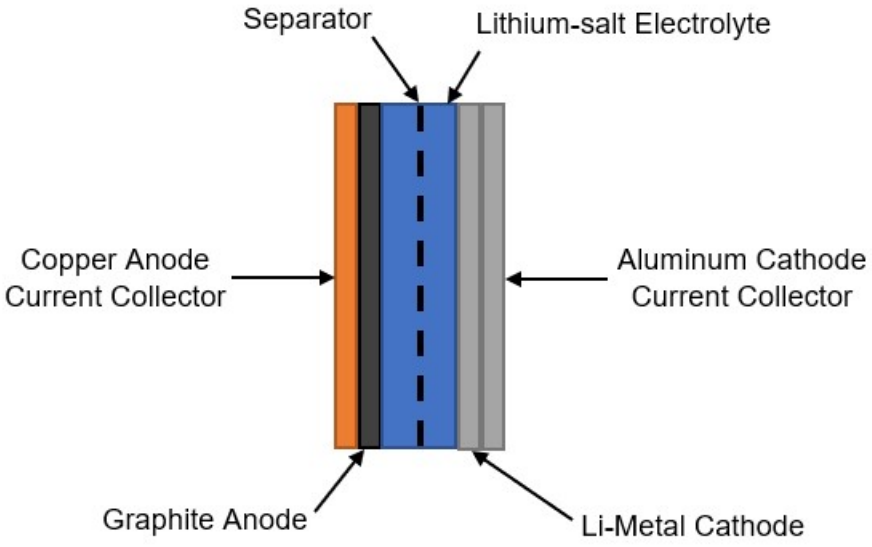

Figure 2.1.1: Li-ion Cell Construction

Aside from the chemical differences that create slight variations among the name of Li-ion batteries, the basic principles of the way the battery behaves is quite similar. All of these chemistries require certain conditions to optimize cycle life, operating temperature, and retain maximum power capabilities. The first and most important characteristic of a typical Li-ion battery, is a maximum and minimum voltage boundary. Usually the maximum voltage is 4.2V and minimum is 2.5V. The current limits depend on the internal resistance of the battery and temperature boundaries of that chemistry but the optimal temperature of Li-ion batteries is 25°C

to 55°C [24],[25]. Outside of these boundaries the cell can begin to see reduced capacity, reduced charge capabilities without affects on cycle life, or faster rates of cell aging. Another aspect to the characteristics is the health of the cell. This is called the State of Health (SOH). The SOH of a cell is a measure of the age of the cell and it uses the capacity of the cell to consider the aging that has occurred as well as other factors such as internal resistances and other chemical differences. In this context the SOH will only be a determined by the comparison of discharged capacity to the datasheet discharged capacity. It uses the initial capacity of the cell when new which is considered 100% SOH. The End of Life (EOL) of a battery cell is considered to be the point at which the battery has 70-80% of its original capacity and this is when the SOH is 0% [26]. The aging of cells has many different effects on the characteristics of the battery itself. These include the capacity of course but also the internal resistance, maximum charge and discharge power.

The next element of the battery is the battery model as seen from the actual terminals of a cell. Since there are many mechanisms in a battery cell, the way the battery behaves at the chemical level is not the same as the way we see the battery at the terminals. Another perspective on the battery which is very important, especially in the aspect of designing a control system for electrical implementation in a system, is the way it reacts electrically. This is usually demonstrated with a general electrical model as seen in Figure 2.1.2.

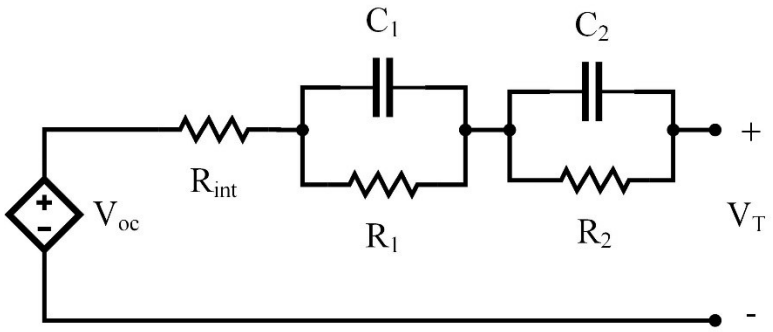

Figure 2.1.2: Li-ion Electrical Battery Model

In Figure 2.1, the internal resistance is labelled as R_{int}, this is the direct resistance that does not change much with time but does change with cycle number based on multiple aging effects. Alternatively, it does change with SOC in a single cycle and it is a non-linear function that is mostly constant until the SOC is less than 30% where it exponentially increases until some

maximum value when the SOC is 0%. Next in series with that is an RC pair seen as C_1 and R_1, then there is C_2 and R_2. The C_1/R_1 values correspond to the polarization conditions inside the cell and the C_2/R_2 values correspond to the diffusion reactions happening inside the cell [27]. These are still series resistances, but they have a time constant to reach the set resistance because of the parallel capacitance and they relate to the slow-response and fast-response of the battery, respectively. The final component is the actual voltage source which is the open circuit voltage (OCV). This is the true cell voltage and represents the accurate SOC when no load is placed on the terminals of the cell.

The charging of Lithium-ion cells is another important task that relies on the characteristics of lithium batteries. The standard charging method for charging lithium batteries is called Constant-Current Constant-Voltage (CC-CV) charging. Lithium batteries have limits on charging current because of lithium plating on the anode, some doped or different anodes are seen in [28] which can improve charge speed. This region before the maximum cell voltage is called the CC region, hence the constant current which is usually set to the maximum charge current or available charge current from the charger. Once the battery has reached the maximum cell voltage during the CC mode, the charge mode then turns to CV to stop the battery from overcharging (over-voltage) damage from occurring to the cell. The reason CV occurs is because of the internal resistance and other series resistances seen in the model. There is some voltage drop across these resistances. What the charger does is stay in CV mode and as the OCV of the cell increases, the current decreases. Once the charge current reaches a set value the charging is stopped, and the cell is considered to be at 100% SOC. The typical voltage, current, and SOC vs. time curves of a Li-ion cell can be seen in Figure 2.1.3.

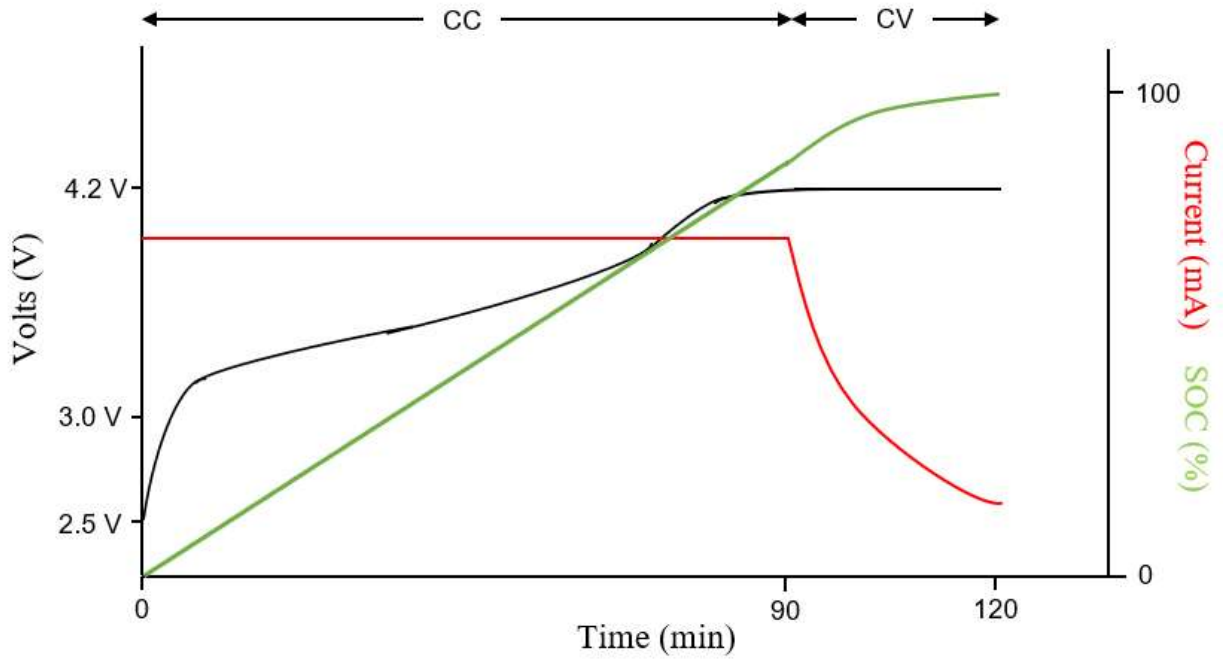

Figure 2.1.3: Li-ion Cell Charge Curves

2.2 SOC Estimation Techniques

SOC estimation techniques are another increasingly researched area. Research is showing that we can have better control and utilization of a battery if we have an accurate understanding of the battery model or accurate understanding of how a battery responds or will respond. There are many ways to estimate the SOC of a cell but there are only a limited number of variables which can be measured on a cell in order to make these estimations. These are namely the current, the terminal voltage, time, the cell temperature, and internal resistance [28]. The goal of all SOC estimation techniques is to accurately estimate the charge remaining in a battery.

2.2.1 Coulomb Counting

Coulomb counting, also known as Ampere-Hour counting is the most common form of SOC estimation used in the industry today, or at least in combination with Open Circuit Voltage (OCV) estimation. The Coulomb Counting technique is an effective, budget-oriented estimation technique that does give a fairly reasonable estimation on the SOC of a battery. The downside of Coulomb Counting however is that if the initial SOC measurement is incorrect then the whole estimation will be incorrect throughout the charge cycle. This can be seen in Figure 2.2.1.

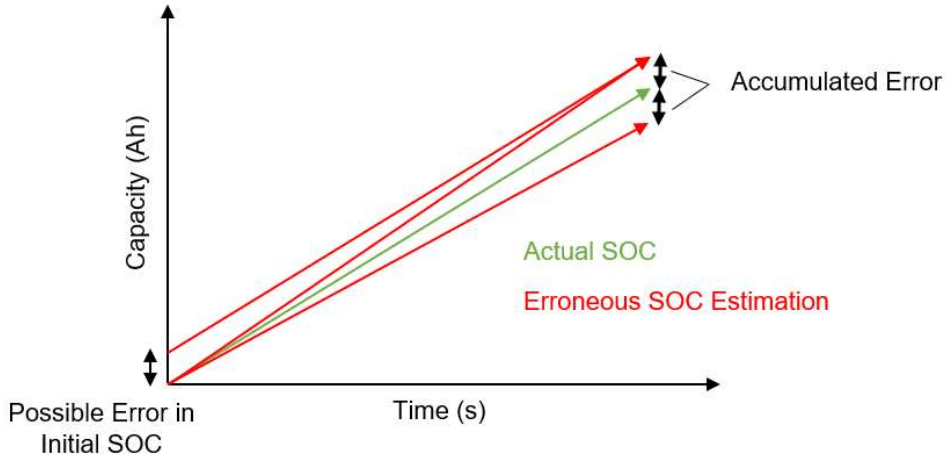

Figure 2. 2.1: Coulomb Counting Error

Another area of possible error is accumulated error through an inaccurate current sensor. This can accumulate error for a larger SOC estimate or can be reading a higher than true current leading to a smaller than true SOC estimate. Another major factor affecting the coulomb counting method is the possible error due to larger currents or varying current through the battery which is lost to internal resistances. As seen in [29] there are some advanced coulomb counting methods that can be used to make more accurate SOC estimated if a model of the battery is acquired. Even if the coulomb counting technique used does take into account some general internal resistance losses, the changing SOH creates changes in the internal resistances. This also shows how the coulomb counting method is a closed loop system so as the SOH reduces, the error will increase [30].

2.2.2 Alternative Direct Measurement Techniques

The alternative measurement techniques include the main measurable variables of a battery to make direct calculations of the SOC. These techniques mainly include OCV or EMF estimation, impedance spectroscopy, and look-up tables. These measurement types are fairly accurate but usually are not realistically implementable in EV applications or require a detailed battery model in order to be accurate.

The first direct measurement technique is OCV estimation of the cell using the terminal voltage of the cell and some trained battery model. Using the battery model, we can relate the discharge current and temperature with the measured terminal voltage. The OCV estimation

method is accurate if a battery model is supplied with the battery characteristics defined and accurate sensing equipment supplied. The OCV measurement method would be even more accurate but the voltage vs. SOC curve is not a linear line as can be seen in Figure 2.2.2. Therefore, the battery model is needed but with enough testing to get the battery model, the OCV SOC estimator is accurate [31]. The figure shows a typical Li-ion discharge curve from 4.2V to 2.5V which is a common operating voltage range.

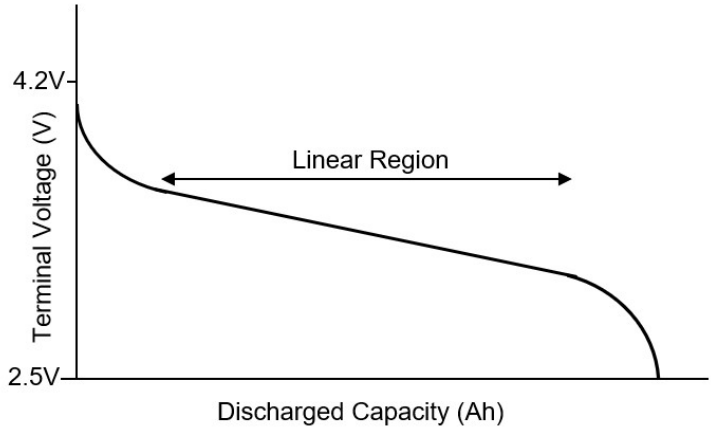

Figure 2.2.2: Lithium-ion Typical Discharge Curve of SOC vs. Voltage

Therefore, the drawbacks of an accurate OCV estimator is the requirement of a lab tested battery model in order to make accurate estimates. Another estimation technique which suffers the same issue, in terms of feasibility, is the standard look-up table. The look up table estimator typically requires the measured current, voltage, and temperature alongside a "look-up" table, made from a tested battery model, to determine the SOC at that point in time. In [31] a very accurate OCV-temperature-SOC estimator was experimentally validated.

2.2.3 Artificial Neural Networks

Artificial Neural Networks (ANN) are the first type of SOC estimator that is very computationally intensive but can be highly accurate and adaptive to SOH changes especially in the non-linear regions. The way ANN work is they take in battery state variables, called the input nodes, those are mapped to hidden nodes, which then combine to give one output. In this case the ANN is used to determine the SOC using measurements on the battery. The ANN is modeled after

the neurons in the human brain, where the inputs take multiple paths simultaneously to reach an output(s). This can be demonstrated in Figure 2.2.3.

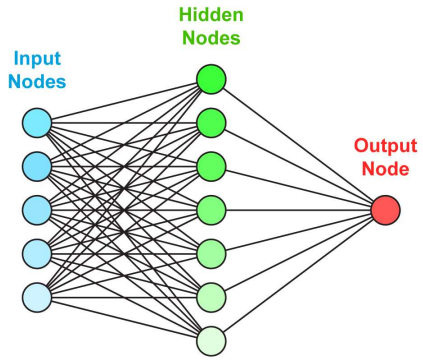

Figure 2.2.3: ANN Network Structure

The way an ANN works is initialized is all node weights are set to 0, when the model is trained these nodes develop characteristic weightings which then create the battery model and can be then used re-currently to give an output which is SOC [33]. And pre-trained battery model can be supplied to skip the training process for a new BMS but will not be as accurate as the original battery the ANN was trained on. This can also be a downside if the variability in battery characteristics is large due to manufacturing imperfections or other disturbances in battery behaviour are present due to the pack design, etc. [34].

2.2.4 Kalman Filters

The Kalman filter is a variable estimation algorithm that uses measurements and a series of related linear quadratic equations to estimate the state of an unknown variable. This technique is very computationally intensive since there are many equations being constantly processed and with comparisons to previous and current variable states to then estimate the state of the new variable. The Kalman filter based SOC estimator is the most commonly researched estimator although it becomes more complex for estimating the SOC of Lithium batteries due to many non-linearities in their characteristics. The most common method of using the Kalman Filter is with the Extended Kalman Filter. Many research articles have been published to estimate the SOC of many Lithium chemistry batteries with both the EKF and other system linearizing methods [35]-[38]. There are also many variations of the Kalman filter to improve the SOC estimate such as the Dual

EKF [39], using the unscented transform to linearize the system [40], and even using other recursion themes to reduce computational load [41]. The Kalman filter based SOC estimator is very promising for future SOC estimators because it is highly accurate, can work well with a simple battery model, is accurate in non-linear regions of the SOC, and most importantly for EV's, it is accurate with dynamic loads. The recurring estimation cycle can be seen in Figure 2.2.4.

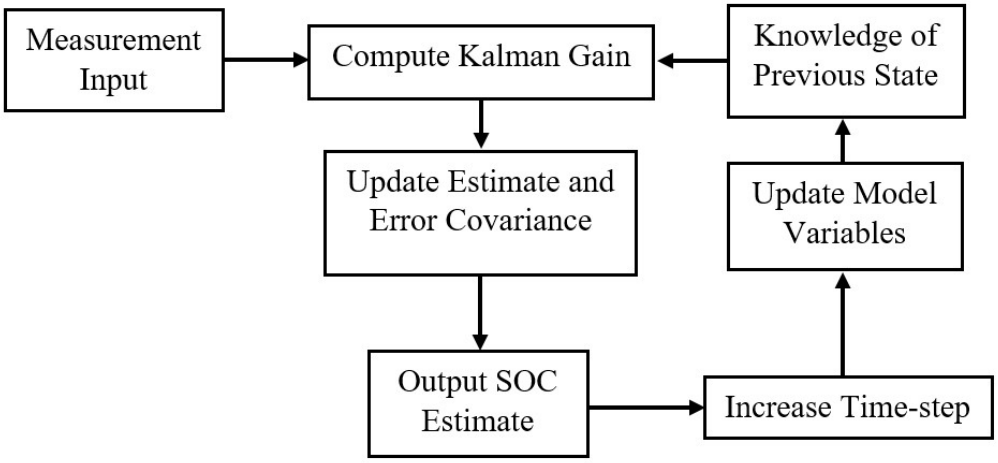

Figure 2.2.4: Kalman Filter Estimation Cycle

The main drawback for Kalman filter based SOC estimators is the very large computational burden. The continual processing of the Kalman algorithms requires a lot of computational power but there are ways to reduce this requirement. The process of polling each cell with a reduced time constant as seen in [41] reduces the computational burden. The use of a simpler battery model such as in [40] can also reduce the computational load. Currently most of these Kalman based SOC estimators are not computationally efficient enough to be realistically implementable in the common MBMS but the industry is pushing research to make the implementation a reality.

2.2.5 Fuzzy Logic

Fuzzy Logic SOC estimators are another computationally intensive SOC estimator. Fuzzy Logic computation works in a similar manner to human thinking, it typically involves different clusters of data and has input variables that have a certain degree of membership to each cluster. This then reduces to "if → then" reasoning which is similar to human thinking. This then goes through a de-fuzzification block which outputs a real value which is SOC in this case. The clusters are separated into two main categories which are "crisp" (certain) and "fuzzy" (uncertain). A

disadvantage like ANN that fuzzy logic has, is the model training, the susceptibility from inaccuracies from external factors that vary from the trained model and require a large computational memory [42]. Overall, the fuzzy logic SOC estimator is not very common for research as an SOC estimator as other estimators are usually more accurate and are not susceptible to such specific models to be provided.

2.2.6 State Observers

There are many other SOC estimators that are based on complex algorithms that are used to estimate the state of an unknown variable using related variables. Most of these other estimators are complex and require lots of computational power. There are Luenberger observer based SOC estimators in [43], the PI Observer [44], and State Vector based SOC estimators [45]. Most of these observers and other methods for SOC estimation are new research areas that are not yet matured for industrial development or tested enough for mass production. They might not continue to be deeply researched areas since most of the common SOC estimators currently require less computational power or provide a more accurate estimate than these observers.

2.3 Standard BMS Cell Balancing

The standard BMS in an EV uses the distributed structure with a PBMS and MBMS. The cell balancing is all done on the MBMS for the cells that the MBMS is monitoring. The industry standard for cell balancing is the switched shunt resistor cell equalizer. This topology is the cheapest, simplest, and has the least complex control requirements [46]. This is why it is the type of equalizer found in most EV batteries today. The shunt resistive equalizer has a very simple control process which is simply, if the cell being monitored has a voltage greater than the others by a set deviance then the resistor is engaged across the cell to discharge it while the other cells continue charging. The power flow with the shunt resistor is very good with no ripple because it is only a resistive load with no fast switching. The shunt resistor circuit can be seen in Figure 2.3.

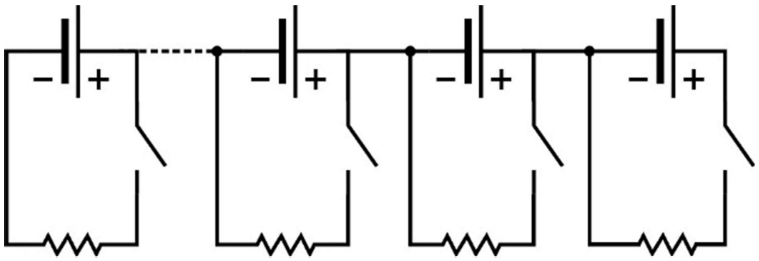

Figure 2.3: Shunt Resistor Equalizer

The BMS continues to engage the shunt resistor during charging until that cell is within a set voltage threshold between all the cells. Another downfall of the shunt resistor topology is the fact that the way this topology balances the cells is by dissipating the excess energy in the highest voltage cell(s) as heat. Due to the heat production the balancing speed is limited to the design of MBMS with concern over the heat dissipation [47]. This heat production also usually takes place on the PCB board of the MBMS itself which is sensitive to the heat affecting other components. The introduction of liquid cooling in EV battery packs does add the capability of also cooling the MBM board or possible use of resistors that are not directly on the PCB board and on a cooling plate. This would allow the use of balancing currents greater than 500mA which would typically correspond to a balancing power of 2.2W or more as the balancing current is usually highest near the full-charge state of the Li-ion battery (4.2V).

2.4 Active Cell Balancing Techniques

2.4.1 Single Capacitor Equalizer

The single capacitor equalizer is the first and most basic capacitive equalizer. The way that it functions is it uses a single capacitor to switch to and store energy from a higher potential cell then switch to a lower potential cell and transfer some energy due to the voltage difference. This topology is also known as the single switched capacitor equalizer or flying capacitor equalizer because it single “flying” capacitor and switches at high frequencies to reduce voltage ripple and increase energy transfer rates. The switching frequency and capacitor capacity are two variables that depict the energy transfer rates (balancing current) for design specifications. This cell

equalizer topology requires a matrix of switches in the series stack of cells, so the capacitor has the ability to connect to any cell in the stack. The relation between switching frequency and capacitor size is that a higher switching frequency allows the use of a smaller capacitor to transfer the same amount of energy [48]. The benefits of a single capacitor equalizer are that it has a basic control algorithm, is cost effective, and has a simple circuit. Some drawbacks it has is that it does not have good control of inrush current to the capacitor from the cell and as the voltage difference between cells becomes smaller, it becomes harder to accurately balance the cells. The topology for the single capacitor equalizer can be seen in Figure 2.4.1.

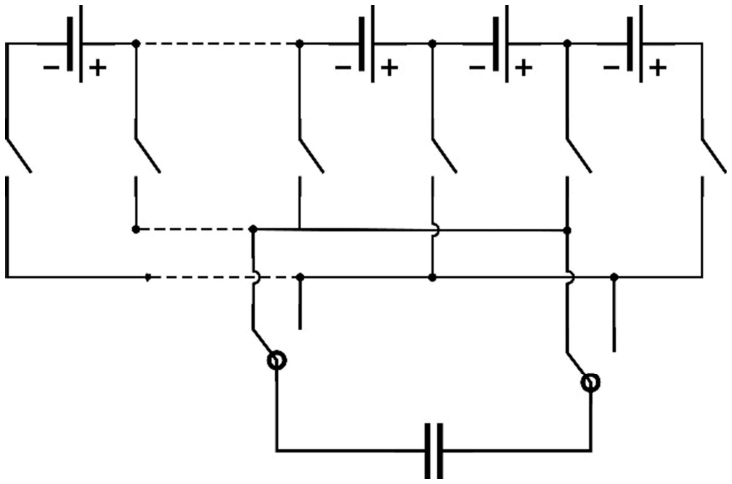

Figure 2.4.1: Single Capacitor Equalizer

2.4.2 Switched Capacitor Equalizer

The switched capacitor equalizer is the second capacitor-based equalizer with the only other capacitor-based equalizer being the double-tiered switched capacitor. The functionality between all of the capacitor-based equalizers is the same. With the basic principle being that the voltage difference between cells allows a capacitor to charge and discharge between cells to transfer some energy to then balance them. The difference between the single capacitor equalizer and switched or double-tired switched capacitor equalizers is that the single capacitor equalizer is capable of directly transferring energy from the high potential cell to the weaker potential cell. The switched capacitor equalizer can only transfer energy between neighbouring cells so to move

energy down the stack, the energy needs to transfer through all of the cells in between the two cells being balanced [15]. The standard switched capacitor equalizer can be seen by Figure 2.4.2.1.

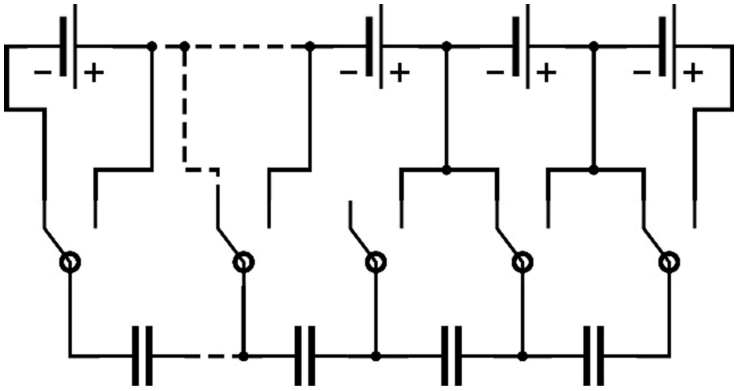

Figure 2.4.2.1: Switched Capacitor Equalizer

The double-tiered switched capacitor equalizer is an improvement on the standard capacitor equalizer. This topology uses a second level of capacitors which now allow energy to be transferred between every two cells and not only neighbouring cells. In [16] the comparison between the standard switched capacitor equalizer and double-tiered capacitor equalizer is made. The findings were that because the double tiered capacitor equalizer can transfer charge between cells and skip one cell in-between the double-tiered capacitor equalizer is capable of faster balancing speeds. The double tiered switched capacitor equalizer can be seen in Figure 2.4.2.2.

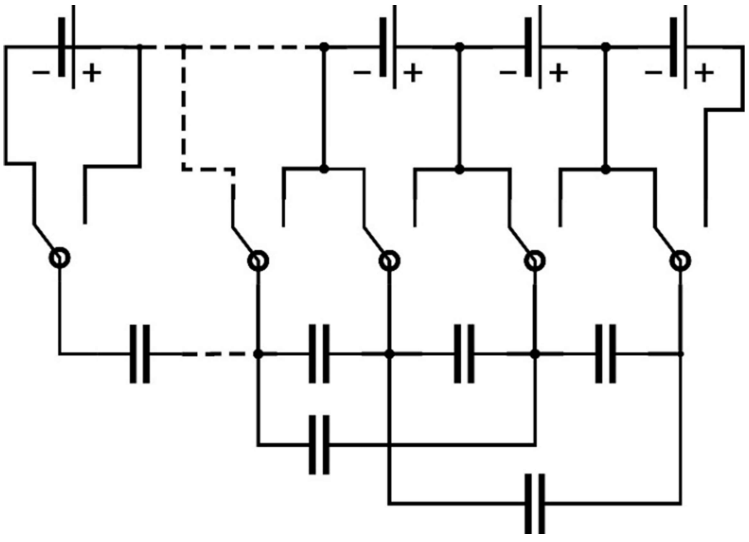

Figure 2.4.2.2: Double-Tiered Switched Capacitor Equalizer

Another benefit is that component stress is reduced with the double tiered capacitor equalizer. An example of the difference in balancing times is shown in [14]. It took a single capacitor equalizer 20 hours to balance two 32Ah cells with a 500mV difference down to a 50mV difference. With an EV this is an unacceptably long period of time because with aging this is a realistic scenario and with this amount of balancing time, it would take 20 hours for the CV portion of charging to occur in an EV battery. In [16] it is seen that with a 50% increase in capacitance of the double-tiered capacitor, the equalization time would be 25% of the switched capacitor equalizer. Therefore, if this applies to the 32Ah cells with 500mV difference, the balancing time should be approximately 5 hours which is far more acceptable. The main drawback of switched capacitor equalizers is the same as the single switched capacitor equalizer as well as a longer balancing time for a series stack of cells where there are two outliers with voltage imbalance.

2.4.3 Single Inductor Equalizer

The single inductor is another take on the single capacitor equalizer with the difference being that the capacitor is replaced with an inductor. The basic principle of operation is also the same with the inductor switching from the higher potential cell and to the lower potential cell. The operation principle of the single inductor equalizer actually has a similar operating principle as a buck-boost converter operating in discontinuous conduction mode [17]. The energy transfer characteristics are also then similar to the buck-boost converter in terms that instead of directly connecting to the device and waiting as what the single capacitor equalizer does, there is now some duty cycle required for control. This now gives more control of the output voltage because of the variable duty cycle of the switches. This does also lead to a drawback of this equalizer which is the control then becomes difficult and over-voltage situations can occur, which would damage Li-ion cells. The single inductor equalizer is shown in Figure 2.4.3.

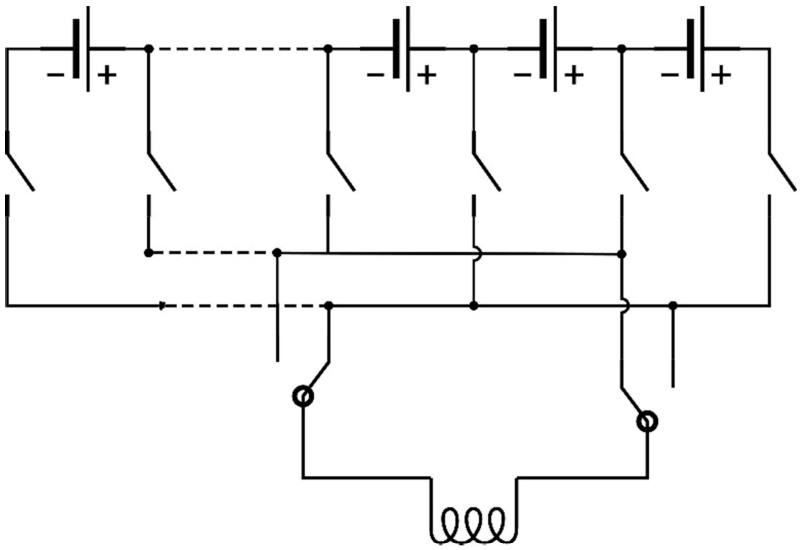

Figure 2.4.3: Single Inductor Equalizer

2.4.4 Switched Multi-Inductor Equalizer

The switched multi inductor is another take on the switched capacitor equalizer. The multi inductor however has many characteristics like a cuk converter. The inductors are located between each cell with a switch then connecting the string of inductors. This can be seen in Figure 2.4.4.

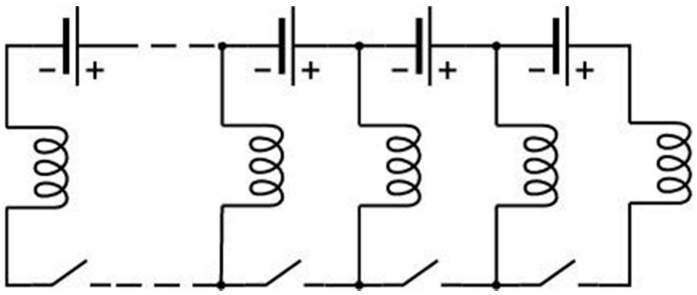

Figure 2.4.4: Multi Inductor Equalizer

The use of inductors allows a smooth current flow between cells but like the single inductor equalizer, the voltage control becomes complex with relations to the duty cycle of the switches. Like the switched capacitor equalizer this topology is only capable of transferring energy between neighboring cells, so the energy must flow through all of the cells between the cells being balanced. The efficiency of this equalizer is very good however with about 85% efficiency in the 1.5A to 5A

of balancing current region [18]. The complexity of current control using the duty cycle of all the switches is ultimately the downfall of this equalizer topology. As well as the balancing time being increased due to having to move the balancing current through the cells between the two cells being balanced.

2.4.5 Buck-Boost Equalizer

The buck-boost converter equalizer is the first DC-DC converter-based topology. This topology is quite broad as there are many variations of the buck-boost converter that can be applied. The layout of this equalizer is a bunch of series connected converters in a string, so the balancing current can then only travel among neighbouring cells. This can be seen in Figure 2.4.5.

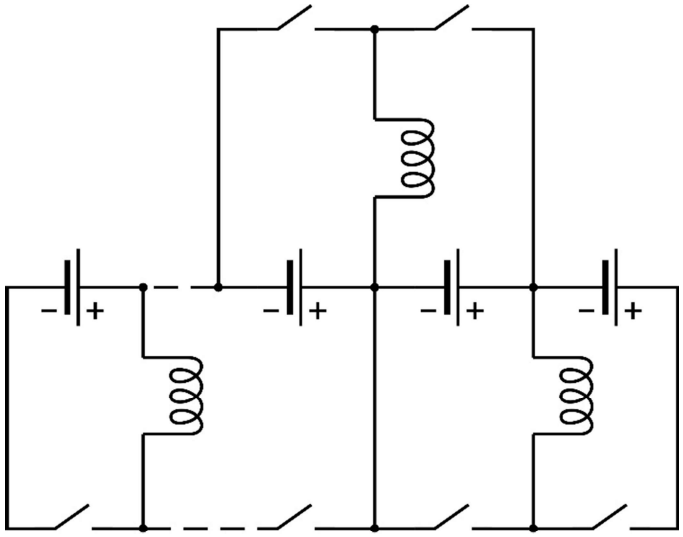

Figure 2.4.5: Buck-Boost Equalizer

The converters seen in Figure 2.4.5 are a simplified outline of the buck-boost converter including the main components which are the inductor and switches but excludes the smoothing capacitors. The operation of the buck-boost converter uses the same operating controls as a typical buck-boost converter. It is just applied to a cell equalizer in this situation. The control aspects of the buck-boost converter are explained in [49]. The configuration of this equalizer are many buck-boost converters which are connected to two neighbouring cells. This then means that the way this equalizer balances the cells is by moving the energy from the higher potential cell to the weaker

potential cell by activating all of the equalizers between those two cells. Similar to the multi inductor equalizer this also reduces balancing speed. The even with the higher number of components and converters, the efficiency of the buck-boost converter is high so the losses even through multiple converter may not be very high. The very accurate control of voltage and current with the buck-boost converter is an advantage for low voltage differences between cells or when a large balancing current is required. There are also buck-boost converter-based equalizer topologies that can also transfer energy from the cell to the whole stack which can then reduce the number of switches and allows equalizer operation without transferring the balancing energy through the stack [19].

2.4.6 Cuk Equalizer

The cuk converter equalizer is another DC-DC convert-based equalizer similar to the buck-boost equalizer. The cuck converter can increase or decrease output voltage like the buck-boost converter. The operation of cuk converter can be bi-directional as well with a symmetrical converter that is symmetrical by the coupling capacitor. The cuk converter also has an inductor on the input and output so the current flow is very smooth as well as a low voltage ripple [50]. A drawback of the cuk converter is the complex control. The two switches are the controlling parameters and there is a complex relationship between the duty cycle and output voltage. The cuk converter can also be fairly expensive because of the higher parts count which include: 2 switches, 2 inductors, a coupling capacitor, and 2 smoothing capacitors. The sizing of these components also affect the current and voltage ripple. A simplified cuk equalizer can be seen in Figure 2.4.6.

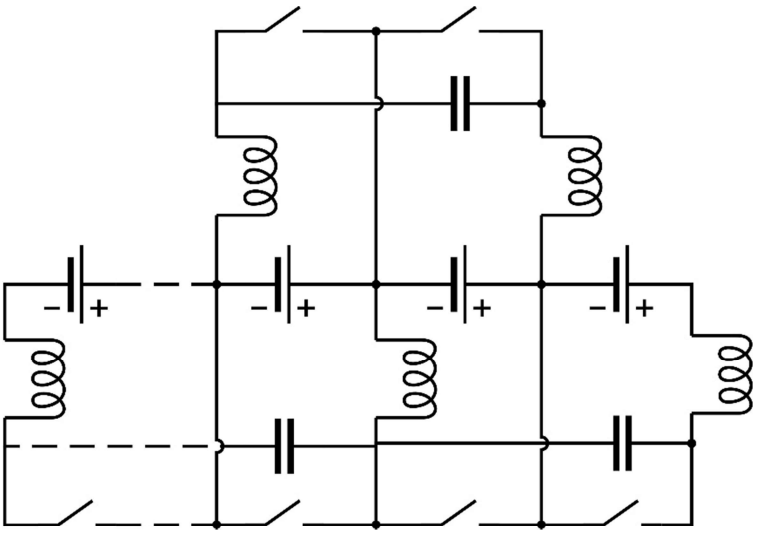

Figure 2.4.6: Cuk Equalizer

The cuk converter is an even more efficient converter over the buck-boost converter and has high current capability for fast equalization times which is required for EV applications. The drawbacks of the cuk converter are complex voltage and current control, larger physical size, and relatively expensive topology. A multi-stacked topology such as in [19] can greatly reduce the size and cost while increasing balancing speed and efficiency. This would be a good area for future research.

2.4.7 Forward Converter Equalizer

The forward converter is a standard transformer-based DC-DC converter. This cell equalizer uses a special multi primary single secondary transformer. The configuration can also use multiple single primary single secondary transformers. The forward converter equalizer operates by activating the highest potential cell above the set voltage threshold to reduce the cell charge thereby balancing the stack [21]. The drawbacks of this equalizer are because of the expensive, large, precise, and heavy transformer required. The forward converter equalizer does however have fast equalization capabilities, relatively simple control, and small voltage/current ripple. The forward converter equalizer is shown in Figure 2.4.7.

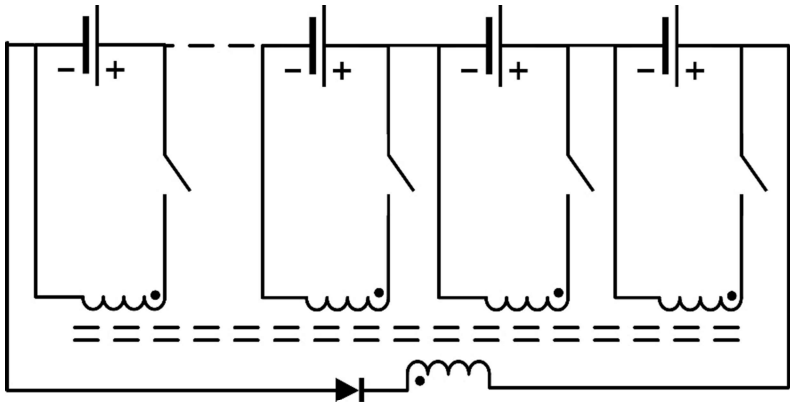

Figure 2.4.7: Forward Converter Equalizer

2.4.8 Fly-back Converter Equalizer

The fly-back converter equalizer is another transformer-based cell equalizer. It uses a single primary multi secondary transformer but like the forward converter equalizer, can also use multiple single primary single secondary transformers. This converter operates by switching current through the primary which then redistributes the magnetic through each of the secondaries. The balancing occurs by having difference reluctances on each of the secondaries. The different reluctances are due to the different cells voltages and the cell with the least voltage will get the most current thereby balancing the cells during the charging process [51]. The fly-back converter equalizer has the same drawbacks and advantages as the forward converter equalizer but slightly different operating principles. The fly-back converter is shown in Figure 2.4.8.

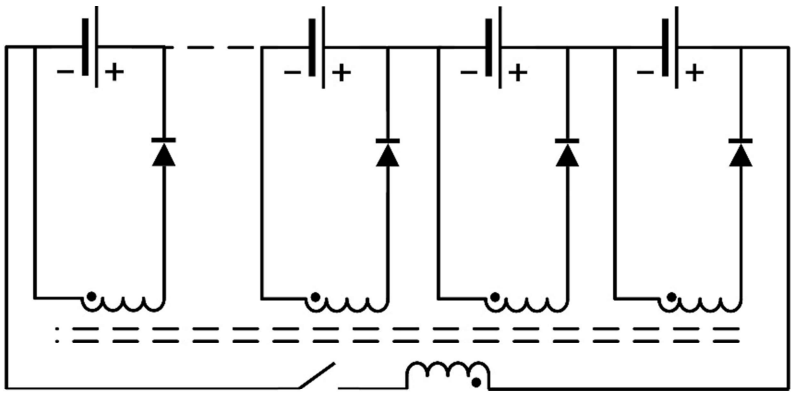

Figure 2.4.8: Fly-back Converter Equalizer

2.4.9 Quasi-Resonant ZCS Equalizer

The Quasi-Resonant Zero Current Switching (QRZCS) equalizer is a DC-DC converter-based cell equalizer. The topology of the QRZCS topology is the same as the buck-boost topology but with the addition of the resonant circuit. The QRZCS equalizer is also the most complex equalizer because of the large number of components and the complex control of the converter. The resonant circuit is an LC pair that requires special controller design that includes the resonant start control. The QRZCS converter has a very high efficiency of 96% as compared to the standard buck-boost converter because of the soft switching [20]. The operation of the QRZCS converter is very much the same as the buck-boost converter but includes close monitoring of the switching frequency and resonance in the circuit. The QRZCS equalizer has good equalization speed, excellent efficiency, and still has a relatively small size, even with the additional inductor and capacitor over the buck-boost converter. The drawbacks include the complex control and cost from many components. The QRZCS equalizer is shown in Figure 2.4.9.

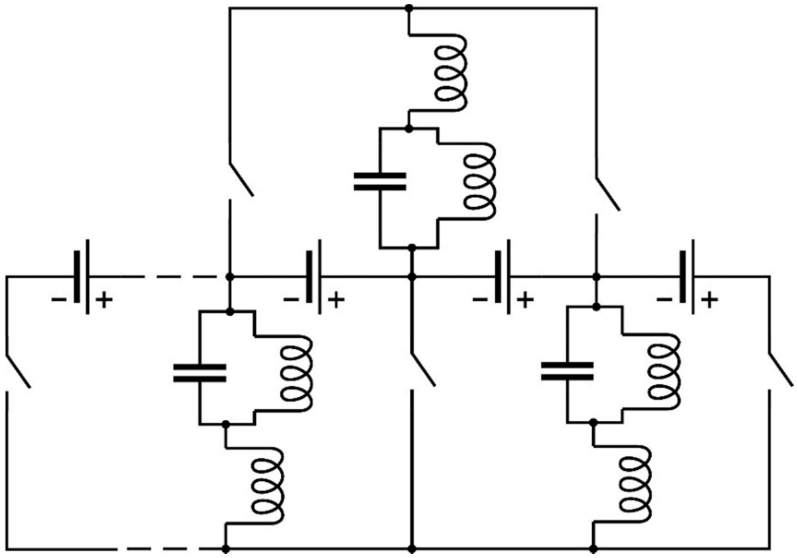

Figure 2.4.9: QRZCS Equalizer

2.4.10 Active Equalizer Comparison and Analysis

The design features and control aspects are the main targets for comparing all the different active cell equalizers. The physical characteristics being considered are manufacturability, size,

and cost. The electrical and control characteristics being considered are the equalizing speed, current/voltage ripple, control complexity, and cell to cell energy transfer efficiency. The equalizing speed is the speed at which the higher potential cell can balance with the lower potential cell to the voltage difference set in the BMS. The control complexity is how difficult it is to control the converter in order to balance the cells properly. The simpler the control scheme is, the better the score. The energy transfer efficiency is the efficiency achieved between transferring energy from the higher potential cell to the lower potential cell. Due to high frequency switching in all the converter, there is some voltage and current ripple generated. In the comparison this is considered as the power flow. As what was seen with the battery model, there is a short-term capacitance related the battery model. This voltage ripple causes increased cell heating due to the actual ESR in that capacitance, increased cell heating reduces the cell life as seen in [52]. The implementation in EV's and with that the comparison topics are aimed at the balancing time, which can slow down the charge time, the cost of the converter, which impacts the battery pack cost, and the effects of the converter balancing on the battery cell life. All of the cell equalizers are compared in Table 1. The comparison is based on the important factors applying to EV's.

Equalizer Topology	Speed	Control	Efficiency	Power Flow	Manufacturability	Size	Cost
Single Capacitor	3	3	3	2	3	2	3
Switched Capacitor	2	3	3	2	3	3	3
Single Inductor	3	3	3	3	3	2	3
Switched Inductor	3	2	4	4	2	3	2
Buck-Boost	3	2	3	4	2	2	3
Cuk	3	2	4	4	2	2	2
Forward Converter	4	3	4	4	1	1	1
Fly-back Converter	4	3	4	4	1	1	1
Quasi Resonant ZCS	3	1	4	4	2	2	2

Table 1: Cell Equalizer Comparison

In the comparison of the active cell equalizers, 9 of the most basic form of each were compared. As previously stated, there are variations of each of the converters but only the base form was assessed in this comparison. As seen by the speed category and as previously stated, there are many converter topologies that can only transfer energy between neighbouring cells. This

increases equalizing time and also reduces efficiency since the energy is not directly moving from the higher potential cell to the lower potential cell. There are also many different components used in each which factor into the cost and size which is an important feature for EV BMS designs.

The single capacitor and single inductor equalizers have similar characteristics with the capability to directly switch from the higher potential cell to the lower potential. The total cost of these converters is relatively low as the switch matrix which is required can be made from a single component with the series of internal switches. The control scheme of both of these converters is also simple with direct cell to cell switching. The size of both of these converters is also small due to only having two large components rather than multiple large components in series such as the other converters that can only transfer energy between neighbouring cells. The switched capacitor, double-tiered switched capacitor, and multi inductor equalizers are also good options for EV BMS applications although they do have more active components while still having a large number of switches. The control strategy for all these topologies is also not as simple as the single component variants of them mentioned previously.

The DC-DC converter-based equalizers are very efficient and have good power flow characteristics but the higher cost and complex control does hinder their application to EV BMS systems. With the fast equalizing speed required from EV BMS systems because of desired fast charge times, these converters do work well while mitigating cell deterioration from fast balancing speeds because of the smooth power flow these converters supply. If cost and size is less of a concern than heat production and efficiency, then the QRZCS converter would be great option for its very high efficiency while still maintain the smooth power flow.

The transformer-based equalizers also offer smooth power flow, high efficiency, and simple control but they are hindered by the higher cost of the transformer which is required for their operation. This trade-off between the large switch or component count in other converters compared to the single expensive transformer-based converter, may not be a large factor due to the fact that the transformer-based converters have the capability to directly balance the lowest potential cell. One concern that may be present with the transformer is EMI production in relation to other sensitive components on the BMS such as some I2C or SPI digital communications.

In the EV BMS there are many different aspects to the design of the equalizer that can be considered critical over others. Maybe the cost is more important or improving the cell life by having less voltage or current ripple. With all the active converters, they are capable of balancing the cells voltages and have different ways of doing so. With the EV BMS and pertaining to what is required to push EV's to become adopted faster, the cost and equalizing speed are considered to be the most important traits. With faster equalizing speeds the CV portion of charging can be reduced and with discharge balancing the range can be increased without having to change the cells. This of course, must all be balanced by the resultant cost of the equalizer topology.

2.5 Summary

This chapter briefly discusses the characteristics of the Li-ion battery and the SOC, SOH, battery model, and different aspects related to implementation in EV's. Many of the standard SOC estimation techniques used by the BMS were explained with different characteristics and abilities to accurately estimate the SOC of a Li-ion cell. As seen the Li-ion battery characteristics are usually non-linear, especially when a dynamic load such as EV is applied to the battery. Thus, the desirability to accurately know the SOC of the cell is very useful in accurate range estimation and optimizing the use of battery capacity. The majority of cell equalizers used in the BMS system to balance series cell voltages was also discussed and compared with many of the different advantages/disadvantages in EV implementation. The standard cell equalizer was also displayed, and it is quite obvious that previous and most EV BMS systems in the past and present are focused on the cost and simplicity for the BMS system. However, with range and charging speed becoming an ever-greater desire to push EV's to be adopted, the use of active cell equalizers and more complex SOC estimation will become evident.

Chapter 3

Discharge Cell Balancing

During cell discharge, from something such as driving an EV, the series cells in a battery pack can have different voltages. This can arise from many different factors such as manufacturing processes, material impurities, differential heating in a battery pack, and differential aging among cells. The BMS in typical EVs will consider a battery to be at 0% SOC when the first cell reaches a cut-off voltage. As the cells drift apart in capacities the weaker cell reaches this cut-off sooner. This chapter focuses on BMS implementable solutions to increase the useable capacity of a battery and improve the overall life of a battery pack.

3.1 Discharge Balancing

Most BMS cell equalizers focus on the balancing of cells during the charging process. This is done mostly during the CV region of the charge curve where the charging current begins to slow down and the difference in cell voltage is evident. In an EV there is a large battery pack, and, in the battery, there are cooling channels for a liquid cooled system. The liquid cooled battery cooling system is common on EV's because it makes the battery pack size much more compact than an air-cooled battery pack. The liquid cooling system in most EV's is not optimized for minimum temperature gradient so there is some deviation from the coolant input to the coolant output. This creates a temperature gradient from the cells near the input to the cells near the output. Corresponding with this over the life of the vehicle there will be some SOH gradient that shifts from cooler healthier cells to hotter weaker cells. In [53], tests between identical cells cycled under the same condition were conducted with the only difference being the cell temperature. It can be seen that cells cycled at 25°C and 60°C undergo difference aging characteristics. The cell cycled at 25°C did not see any capacity loss after 140 cycles but the cell cycled at 60°C lost 65% of its capacity after the same 140 cycle test. The resistance was also much higher due to growth of a high resistance SEI layer which forms over the cathode.

This now brings up the difference in the resistance between cells which as previously seen is the main cause for resultant capacity deviation in series cells after a charge or discharge cycle. Therefore, in a cycle the difference between the terminal voltage is a result of capacity and internal resistance difference. This also means the efficiency of the cell with the higher internal resistance is lower than the one with lower internal resistance. The difference in internal resistance is primarily due to the difference in SEI layer growth because this layer is not very conductive [54]. The SEI layer on the anode of the Li-ion cell can be seen in Figure 3.1.1.

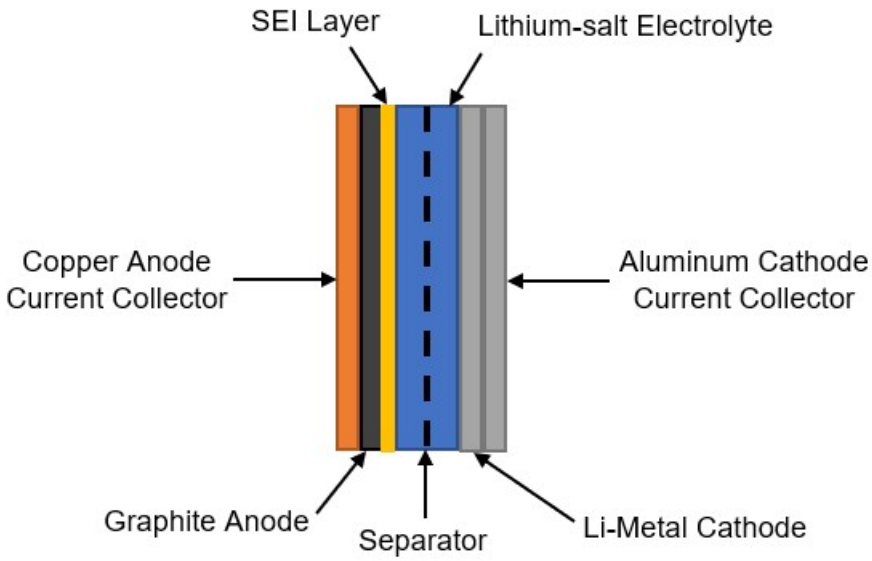

Figure 3.1.1: Cell Construction with SEI Layer

In standard BMS systems found in EV's today, the focus is only on charge balancing. This is partly because the focus has been on the cheapest possible BMS design and this incorporates the standard resistive cell equalizer. The resistive cell equalizer is only really useful in the charge balancing area otherwise there is no point in dissipating energy for the strongest cell near the end of discharge because this will just waste more energy without increasing the useable capacity at all. As detailed previously the standard resistive cell equalizer is also not very fast at equalizing cells because it is limited by heat production. To be capable of discharge cell balancing this means that an active cell equalizer must be applied, one that is capable of transferring energy from the higher potential cell to a lower potential cell. This transfer of energy can happen from a single higher potential cell to a single lower potential as seen in Figure 3.1.2 or can be from multiple higher potential cells to multiple lower potential cells as seen in Figure 3.1.3.

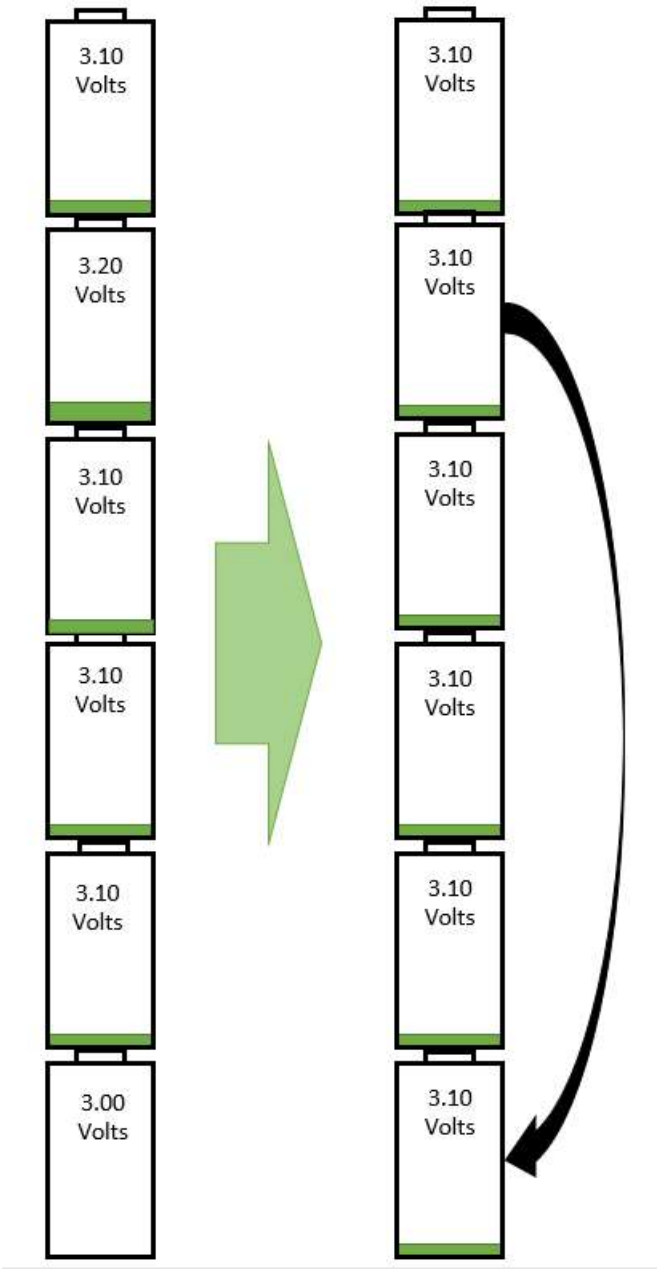

Figure 3.1.2: Discharge Balancing with Single Lower Potential Cell

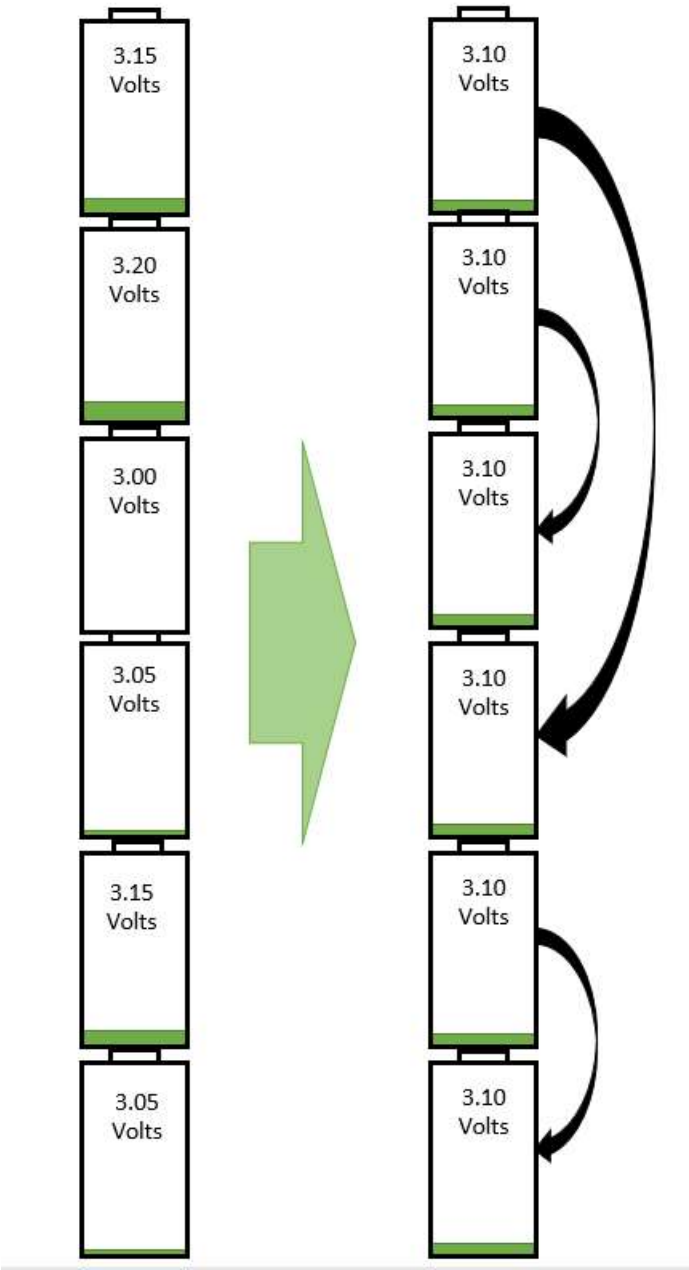

Figure 3.1.3: Discharge Balancing with Multiple Lower Potential Cells

As a result, because there is a difference in capacity and internal resistance, the series cells are unbalanced if the cells are charged or discharged. Also, because the standard BMS has a set cut-off voltage at which it considers the battery to be at 0% SOC, if the lower potential cell is assisted by drawing more current from the higher potential cell then the amount of total useable capacity will be increased. The capacity of the battery is now not limited by the capacity of the

weaker cell but rather it is closer to the average of all the cells in the series stack. This is because the BMS is now making the otherwise un-used capacity in the stronger cell, now useable. Of course, there is no linear relationship between the drawn current, voltage sag increase on the stronger cell, and voltage sag decrease on the weaker cell. The difference in cell voltage is also dependent on the discharge current or the average of the discharge current over time. With greater discharge currents the difference will be greater because of the relation of dissipation power being expressed below.

$$P = I^2 * R \tag{3.1}$$

The voltage difference between cells is a nonlinear function as the voltage curve of any Li-ion cell is non-linear in relation to the capacity and the power dissipation difference between cells is varied by Equation 3.1 which is also non-linear.

The SOH difference that is also generated from cycling and temperature differences can be mitigated with discharge balancing. The capacity fade that results from cycling is due to a parasitic reaction which is causes a loss of active lithium ions. The reaction occurring is a solvent reduction reaction and reducing the Depth of Discharge (DOD) on a cell reduces he time the parasitic reaction occurs for and therefore reduces the capacity loss as a function of cycling [55]. Some relations in the DOD and Capacity vs. cycle can be seen in [55] and [56]. Figure 3.1.4 is presented data from [56] that relates the Capacity (%) and Cycle number for different DOD regions.

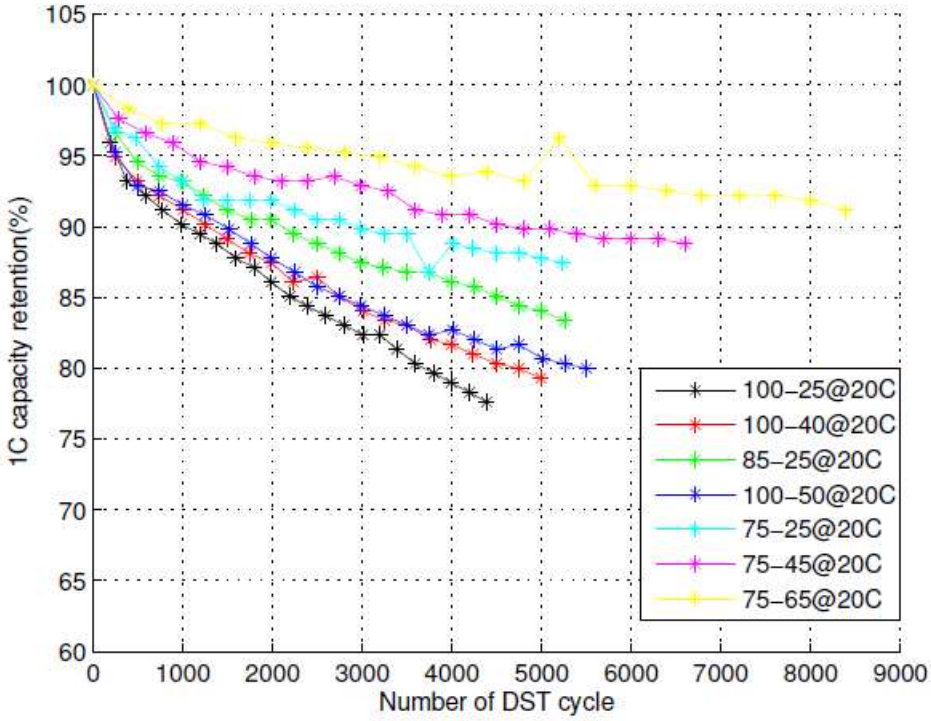

Figure 3.1.4: Depth of Discharge vs. Cycle Life Graph

With the weaker cell in a battery pack undergoing full DOD cycles compared to the stronger cell and the capacity will therefore diminish faster compared to the stronger cells. With cell balancing during the discharge process the load will be increased on the stronger cell and decreased on the weaker cell. With discharge balancing the cell DOD between cells will all be much closer than compared to solely charge balancing which current BMS in EV's implement.

3.2 Applicable Active Cell Equalizers

To carry out the task of balancing the series cells during discharge there are a few characteristics required that must be prioritized. The balancing current must be very high to be able to balance the cells very quickly under a dynamic load because typically under these high discharge rates, the time available to balance the cells is a few minutes or less. The power flow must also inherently be very smooth because during the discharge balancing the balancing current could be very large if the voltage deviation is relatively large. There are also some cell equalizers that are not capable of equalizing cells during discharge or are just not capable of equalizing cells

fast enough. These include the switched capacitor equalizers and the base fly-back converter. The other equalizers that were not considered due to their complex control and high cost are the multi-inductor equalizer and QRZCS equalizer. That brings another important characteristic that is very beneficial for discharge balancing which is direct cell balancing. The capability to balance the higher potential cell to the lower potential will increase efficiency and reduce time which is crucial during balancing under large loads with minimal time available for balancing. In Figure 3.2 (a), (b), (c), (d), and (e), are the five converters that fit best in their base form to perform discharge balancing.

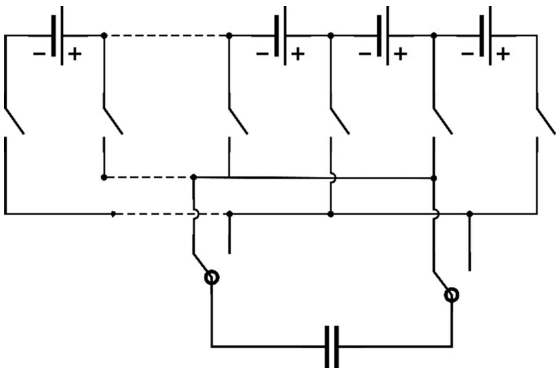

Figure 3.2 (a): Single Capacitor Equalizer

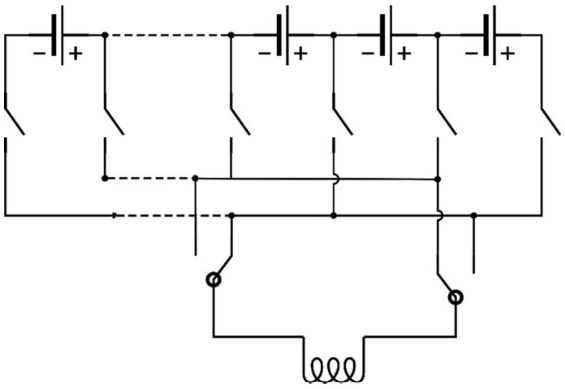

Figure 3.2 (b): Single Inductor Equalizer

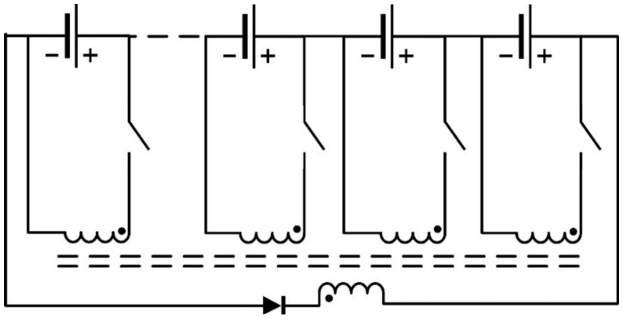

Figure 3.2 (c): Forward Converter Equalizer

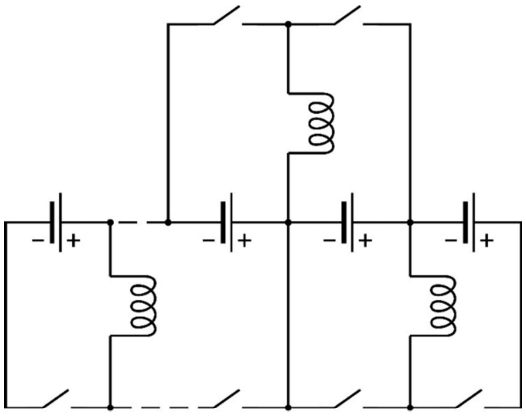

Figure 3.2 (d): Buck-Boost Converter Equalizer

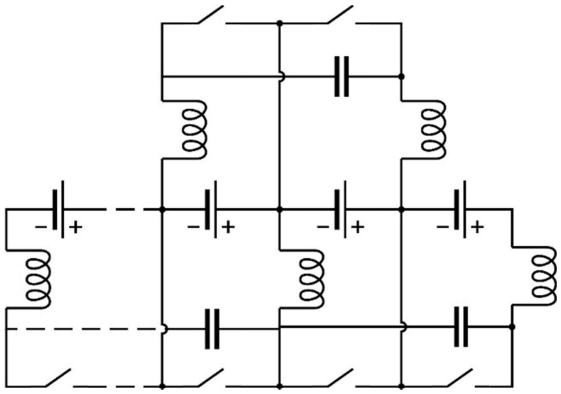

Figure 3.2 (e): Cuk Converter Equalizer

Beginning with the single capacitor and inductor base equalizers in Figure 3.2 (a) and (b). These converters are both capable of discharge balancing and have the most beneficial characteristic for discharge balancing which is being able to balance the highest and lowest potential cells directly. However, with the single capacitor cell equalizer the efficiency of the equalizer is not very great due to the ESR of the large capacitor and control of many high frequency MOSFET's in the switch matrix. The single inductor cell equalizer has many of the same disadvantages, but it does have a higher efficiency which comes at the cost of more complex control. Looking at the forward converter cell equalizer in Figure 3.2 (c) this equalizer is attractive because it is capable of directly discharging the highest potential cells but instead of directly assisting the weaker cell, it discharges that energy into the stack. This does also minorly help the weaker cell but the gain in useable capacity under large discharge currents would not be very beneficial. The final two converters are the buck-boost cell equalizer and cuk cell equalizers in Figure 3.2 (d) and (e) respectively. These cell equalizers both have very similar characteristics in terms of being stacked in series meaning they can only transfer energy between neighbouring cells. Then to balance the highest potential cell to the lowest potential cell, multiple series converters must be activated to balance these cells. This is not a major disadvantage however, because these converters are both highly efficient the total transfer efficiency is still better than something such as the single capacitor cell equalizer. The cuk converter when compared to the buck-boost converter is the better choice for cells. Unlike the buck-boost equalizer the cuk cell equalizer has input and output inductors as well as filtering capacitors. This results in a small current and voltage ripple, making the cuk converter more attractive in the cell balancing application.

3.3 Converter Design

The cuk converter is a good candidate for cell balancing for both charge balancing and discharge balancing. The cuk converter is not a new topology in cell balancing and has been proposed before in [57]. However, the design of this cell balancer was targeted for maximum converter efficiency utilizing zero voltage switching to reduce switch stress and switching losses in the MOSFET. Some other cuk converter-based cell equalizers have been proposed but were all focusing on the efficiency or equalizing speed standpoint of the converters in the application of cell balancing [58,59]. For the proposed converter to be used to conductor discharge cell balancing, the goal is to maintain a good efficiency with minimized stress but more importantly, low current and voltage ripple with high current draws for fast equalizing while not disrupting the voltage sensing of the BMS and reducing cell efficiency from the voltage ripple. According to [60] (Appendix A, HG2 cell datasheet) for every 5A of current difference there is approximately 100mV of change in the voltage sag, which is the voltage drop across the internal resistance and this value is derived from the voltage sag characteristics in the SOC range less than 20%. The LG HG2 is one of the most powerful 18650 format cylindrical cells on the market today therefore the maximum balancing current required would be for a cell such as this. The Voltage vs. Discharged capacity found in [60] is included in Appendix A.

Voltage Ripple	Current Ripple	Maximum Current	Switching Frequency
50 mV ≈ 1%	100 mA ≈ 2%	5 A	37.5 kHz

Table 2: Converter Specifications

The design requirements are determined in Table 2. Using these requirements, the component values and converter characteristics under set conditions can be found. The equations for converter component selection is illustrated in the Power Electronics book by Daniel Hart [61]. From the values in Table 3.3, the maximum voltage ripple is 50mV. This value is selected because during charging the maximum voltage deviation above 4.2V before cell damage occurs is 50mV and because this is an acceptably small voltage ripple for accurate voltage sensing during discharge balancing. The current ripple was selected as a small value and 2% is acceptable considering a

reasonable inductor size and switching frequency. The maximum current as previously stated under worst case scenario for discharge balancing in realistic cases is 5A. The switching frequency was chosen based upon the common frequency selectable from microcontrollers for PWM generation. The general layout of the cuk converter is shown in Figure 3.3.1.

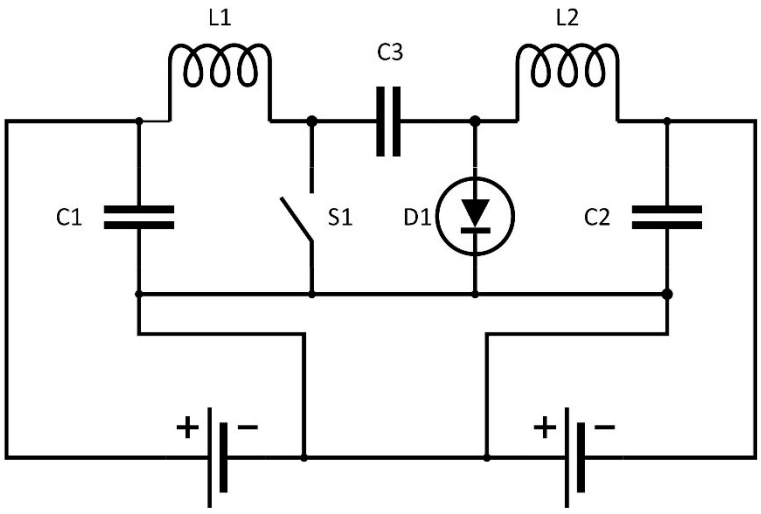

Figure 3.3.1: Cuk Converter General Layout

The first design objective for the cuk converter is the duty cycles to be considered. The maximum and minimum duty cycle are calculated below from the input to output voltage relation calculation.

$$\frac{V_o}{V_{in}} = \frac{D}{1-D} \tag{3.3.1}$$

$$D_{max} = \frac{-V_{in}}{-V_{in}-V_o} = \frac{-3.2}{-3.2-3.0} = 0.516 \tag{3.3.2}$$

$$D_{min} = \frac{-V_{in}}{-V_{in}-V_o} = \frac{-3.0}{-3.0-3.0} = 0.5 \tag{3.3.3}$$

The maximum voltage difference will occur when the weakest cell is near the end of charge which is 3.0V for the Li-ion battery in an EV as this is typically the voltage region where the voltage drop begins to become non-linear. From the calculated duty cycle limits, the inductance values for L_1 and L_2 can be calculated.

$$L_{1,,min} = L_{2,min} = \frac{V_{in,max} * D_{max}}{\Delta i_L * f_s} = \frac{3.2 * 0.516}{0.1 * 37500} = 440.3\ \mu H \quad (3.3.4)$$

The maximum input voltage is 3.2V again with the maximum duty cycle considered as these are worst case conditions. With the inductor values the input and output capacitors values can then be calculated.

$$C_{1,2} \geq \frac{1 - D_{max}}{8 * \left(\frac{\Delta V_O}{V_O}\right) * L_2 * {f_s}^2} = \frac{1 - 0.516}{8 * \left(\frac{0.05}{3.0}\right) * (440 * 10^{-6}) * 37500^2} = 5.862\ \mu F \quad (3.3.5)$$

The maximum duty cycle is again chosen for being the situation at which the greatest voltage ripple will occur. The coupling capacitor is a critical component of the cuk converter and has a voltage swing across it which is an internal variable that can be changed in the design. The voltage swing is ΔV_{C3}.

$$C_3 \geq \frac{V_o * D_{max}}{R * \Delta V_{C3} * f_s} = \frac{3.0 * 0.516}{0.1 * 1.5 * 37500} = 275.2\ \mu F \quad (3.3.6)$$

Another consideration to be made when selecting components is the maximum voltage the component will be experiencing. The maximum voltage can be calculated below.

$$V_{max} = V_{in} + V_o = 4.2 + 4.2 = 8.4\ V \quad (3.3.7)$$

The final design of the cuk cell equalizer is shown in Figure 3.3.2.

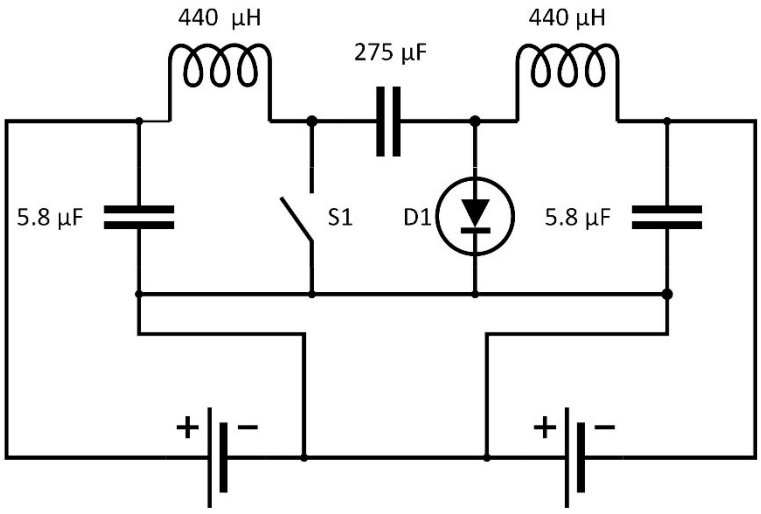

Figure 3.3.2: Cuk Converter Design

With a finalized converter design the cost analysis on the cuk converter can be analyzed. The standard 6-cell passive BMS equalizers account for around 1% of the battery pack cost or less. This is due to very inexpensive resistors and transistors being used for the balancing. The target of 1% comes in comparison to todays conservative measure of Li-ion cell cost coming in at around $200/kWh [3]. This would correlate to $2 of BMS cost per kWh of cell cost, not including the packaging material which would further reduce that percentage of battery system cost. For a cuk converter the costliest components are the inductors and coupling capacitor. The MOSFET's on the large scale of production can be produced quite cheap in comparison and the microcontroller can be similar in cost to a passive equalizer. Estimate numbers for the entire BMS system using the cuk converter active equalizer are approximately 5%. In comparison this is much more expensive than the passive equalizer which is a leading factor why manufacturers do not employ these systems in their batteries. The bulk of the cost comes from the inductors and coupling capacitors making up about 3% of the 5% system cost. The costs were estimated from market value of the calculated component values and ratings. With these findings the BMS equalizer cost per kWh of cells would be about $10 with ballpark market value costs for the calculated component values.

3.4 Converter Simulation Results

The simulation software that was used for simulations is LTSpice. This is a free simulation tool from Linear Technologies with the motive of having mostly just their components readily modelled for simulations. This simulation tool is very effective, easy to use, yet provides very realistic simulations. This software is an excellent platform for simulations of power electronics. In the simulations the Li-ion cell is modelled as a voltage source with series impedance, therefore excluding the first R1/C1 pair that is common with battery model simulations but the goal for these simulations is as follows. Demonstrate the converter is capable of balancing energy from the higher potential cell to the lower potential cell, thereby balancing the voltages to get the required voltage balance. Demonstrate low voltage and current ripple as previously detailed and show any effects the balancing has on the load which is also an important factor in active cell equalizers. The LTSpice simulation circuit is shown in Figure 3.4.1.

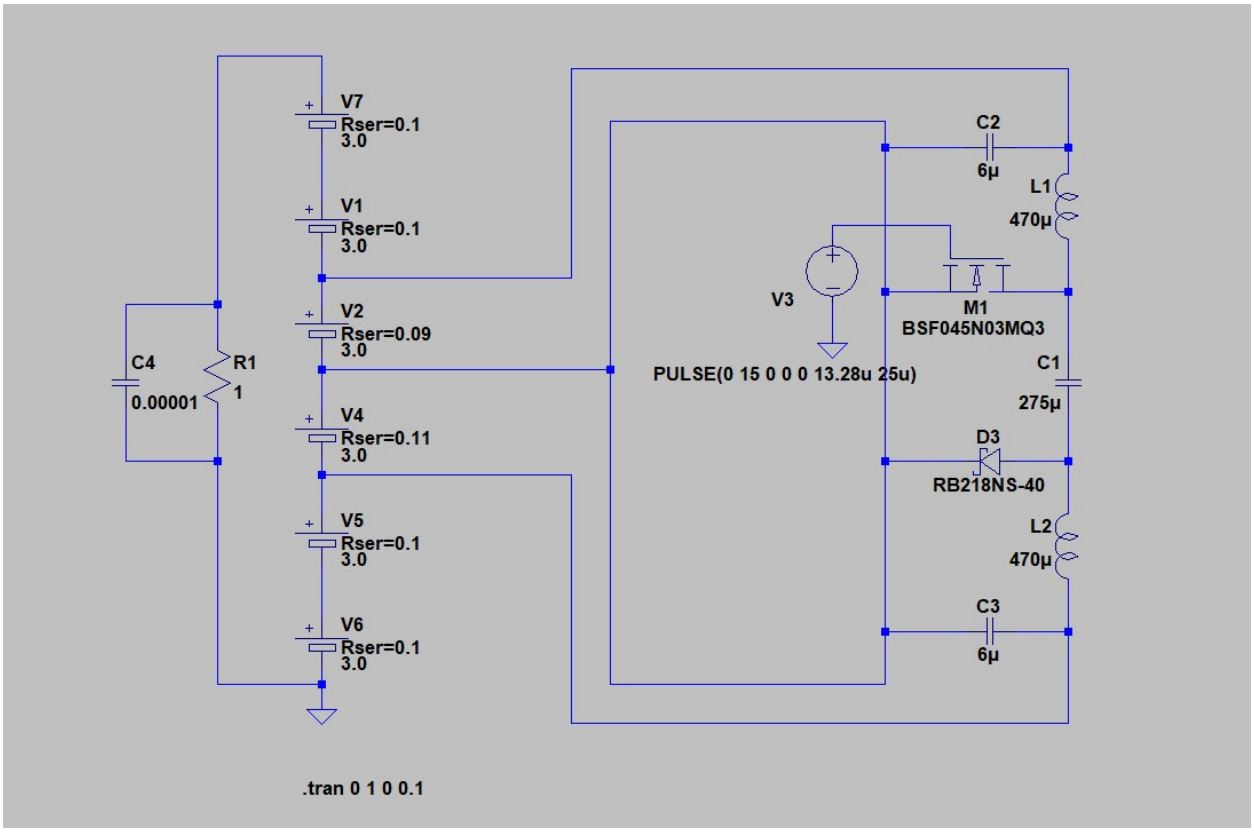

Figure 3.4.1: LTSpice Simulation Model

The first simulation test is to determine the capability to balance the cells during discharge. The cells are modeled with the same V_{OC} but different internal resistances which under a large load will exhibit different terminal voltages.

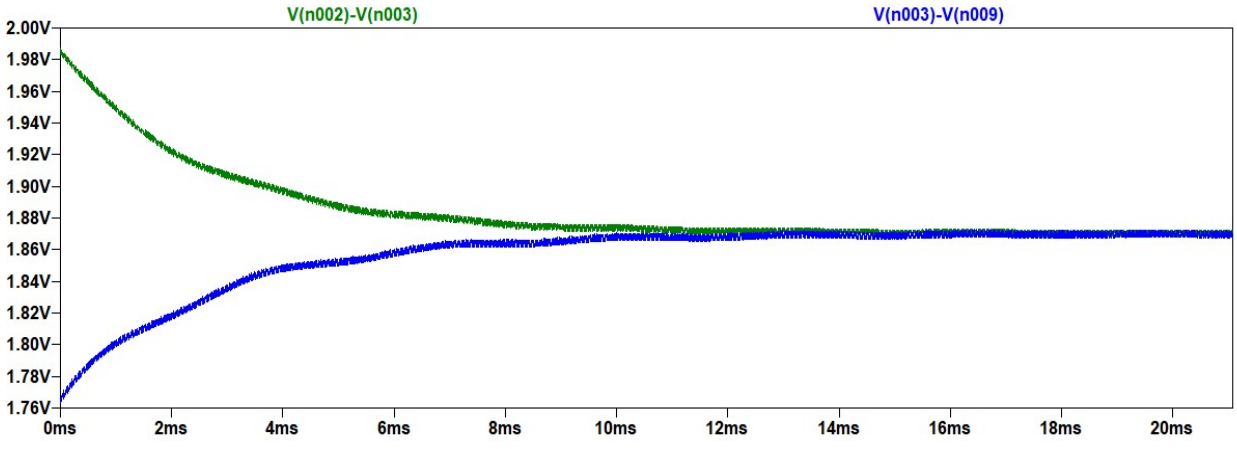

Figure 3.4.2: Balancing Cell Voltages

As explained, the difference in internal resistance for these cells creates the different internal voltage drops and for a 1 Ω load the current ripple, voltage ripple, load current, and steady state cell voltages of the two cells can be seen in Figure 3.4.3.

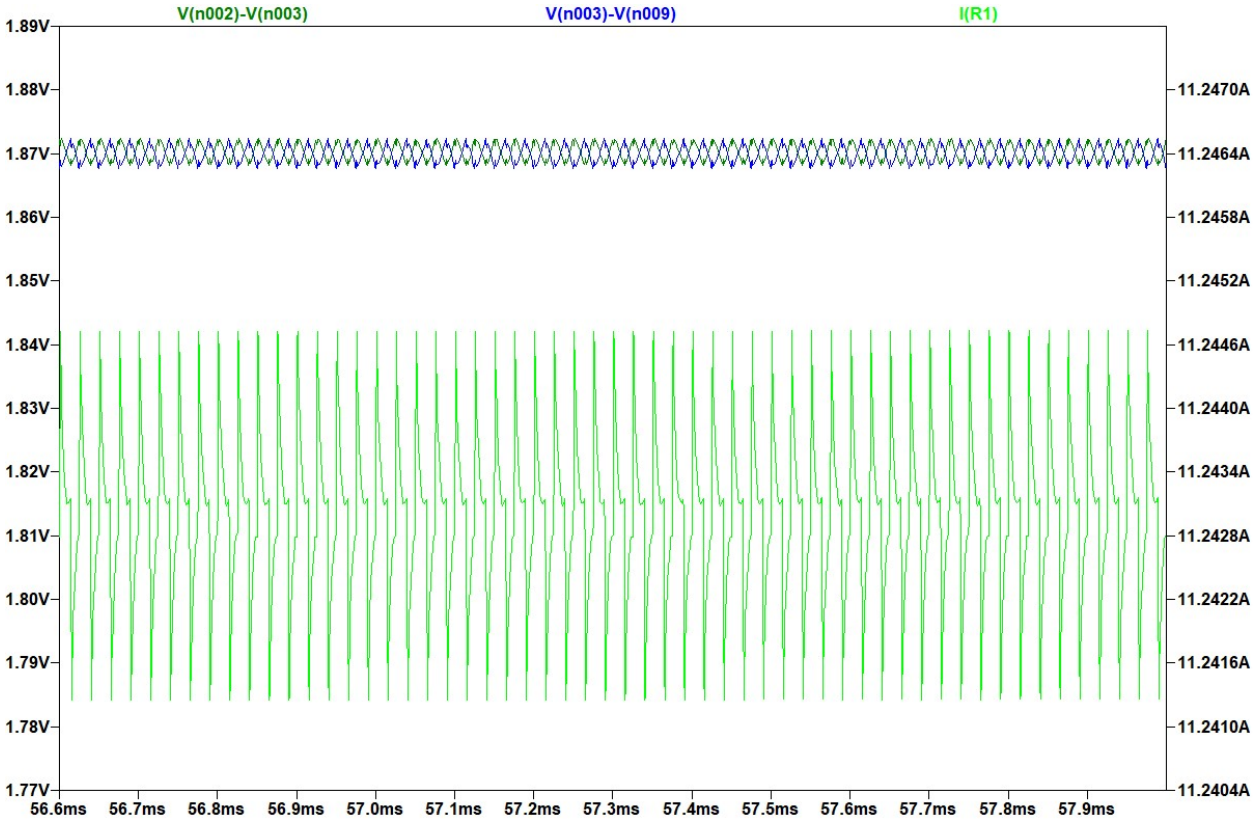

Figure 3.4.3: Balancing Current Ripple and Cell Voltage Ripple

The current ripple seen on the load was a very small 1.5 mA which is excellent and the voltage ripple on both the higher and lower potential cell was only 4 mV. The current seen from the stronger cell and weaker cell as well as their terminal voltages is seen in Figure 3.4.4.

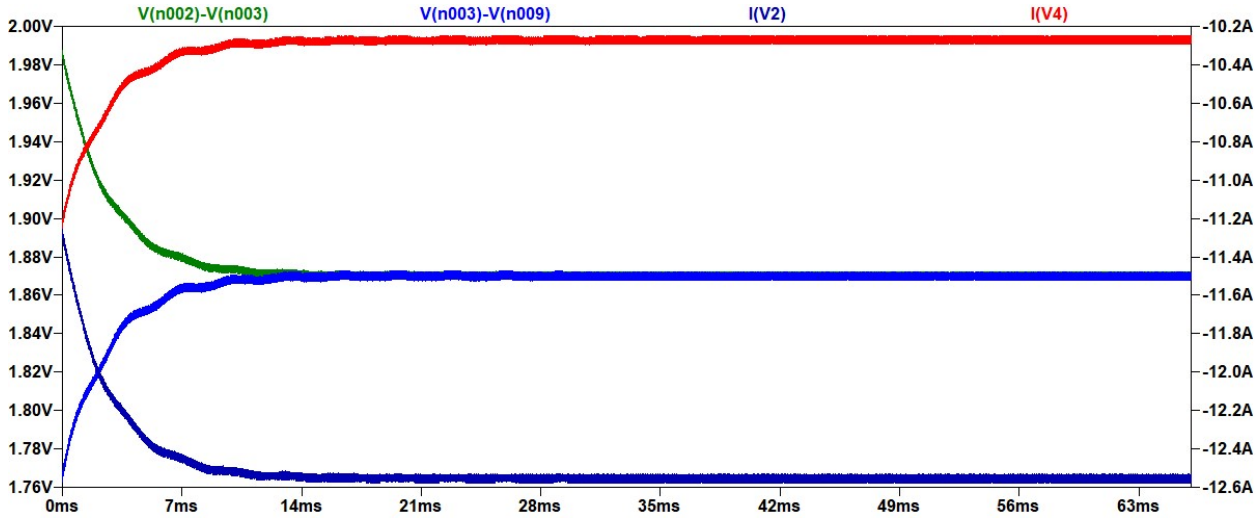

Figure 3.4.4: Individual Cell Load Currents and Voltages

The current drawn from the stronger cell increases from 11.2 A to 12.55 A and the current is assisting the weaker cell reducing the current from 11.2 A to 10.25 A. This shows that the balancing current to the weaker cell is approximately 1.0 A and the input current is approximately 1.35A leaving a 0.35A in current drop due to converter losses. Finally, the voltage and current ripple across the load is shown in Figure 3.4.5.

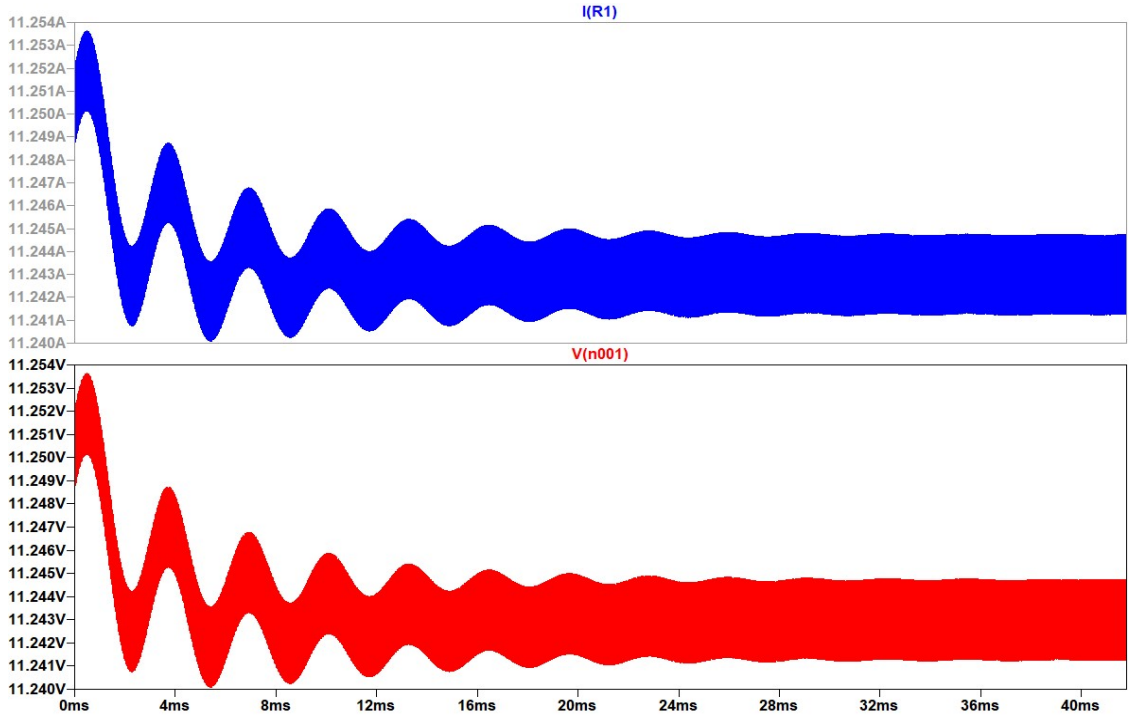

Figure 3.4.5: Load Voltage and Current

With the simulated cuk converter it is shown that it is easily capable of balancing the mismatched cells with a large load of over 10A. The mismatch under these conditions was 200mV as expected but the balancing current required was much less than calculated. It can also be seen that the duty cycle is higher than calculated for, but this is expected when devices with losses are used. The difference in duty cycle was 0.531 in the simulation and 0.516 in calculations.

3.5 Control Strategy

The control strategy for the cell equalizers is quite simple. For neighboring cells, the cell equalizer will vary the duty cycle on the required switches of the converter to draw or give current from the strongest to weakest cells. The control strategy flowchart for a single cell equalizer can be seen in Appendix B. As seen from the flowchart, the discharge balancing will only occur when the current being drawn from the battery pack is greater than or equal to a 1C discharge rate. For some cells the maximum discharge rate is quite low at 2C so the one to two C range is acceptable for discharge balancing. At all points in time the BMS is sensing cell voltages but when discharge balancing for the purpose of discharge balancing, the algorithm uses only the maximum and minimum values to conduct the discharge balancing. It continues to monitor the cell voltages but distinguishes the maximum and minimum values. When the maximum and minimum voltage values drop below 3.1V and the imbalance between those cells is greater than 50mV, the controller begins to drive the cuk converters to discharge the stronger cell and assist the weaker cell accordingly. It continues to control the cuk converters accordingly until the voltages of the maximum and minimum voltage cells is equal or within 10mV of each other. Once these cells are both equal and the voltage drops to or goes below the 3.0V cut-off voltage, the discharge balancing stops, and balancing is complete as well as the discharge cycle of the pack.

3.6 Summary

The implementation and simulation of a discharge balancing capable converter with a control scheme was demonstrated to remedy cell imbalances that appear in cells during discharge. With cells that are new the balancer is less effective due to having much less deviation in capacity and internal resistance as compared to aged cells. Although there is small deviation among new cells, this difference continues to increase as factors such as temperature differences, DOD

differences, and other external factors degrade the cells. The discharge balancer is capable of keeping the capacity and internal resistance differences to a minimum over the life of the batteries. If the deviation still continues to increase the discharge balancer will continue to increase the balancing current to keep the cell voltages balanced up to the maximum balancing current that the simulated converter was designed for. This will still result in a battery that has more useable capacity than a battery pack that does not have a cell balancer. With the simulations for the converters capabilities to balance cell imbalance being verified, the hardware implementation with cells must be conducted to verify the useable capacity increase vs. capacity deviation between cells.

Chapter 4

Discharge Balancing Experimental Results

This chapter deals with the implementation of hardware and Li-ion cells to test the capacity gain that can be extracted with the use of an active discharge balancer. The first set of test data is to be gathered from a standard BMS with charge balancing using new cells to determine the capacity difference when new. Aged cells near EOL will be tested with the same standard BMS for standard BMS useable capacity. The active discharge balancer will then be used on the new and aged cells to determine the useable capacity increase for the given capacity and internal resistance difference between cells. This chapter outlines all the hardware implementation of the standard and active discharge balancers with test data on new and aged cells to determine the increase in useable capacity.

4.1 Test Equipment, Li-ion Cells, and BMS

The test equipment to be used is comprised of the cells to be tested, the 18650 cylindrical cell holders, the standard BMS, the active discharge balancer, DC power supplies, an oscilloscope, and the CC load. This equipment is everything necessary to charge the cells, protect and maintain the cells, discharge the cells, and record test data. The cells to be tested are aged Panasonic NCR18650B cells and the new LG Chem HG2 cells. The 18650 cylindrical cell holder was an in-house built cell holder capable of over 30A of current per cell. The cell holder was built-in house due to a lack of 18650 cell holders that are capable of the high discharge currents which modern cells such as the HG2 are capable of. It also has other features such as 10A capable balance ports for active cell balancer connections for lab testing as well as low current voltage sense ports for BMS and other voltage sensing equipment. The standard BMS is an Energus Tiny BMS s516-30A. This BMS is capable of monitoring, protecting, and charge balancing 4 to 16 series cells. It is also capable of 150mA balancing current, 30A continuous cell discharge and 60A peak cell discharge [62]. The active balancer consists of the converter designed in Chapter 3 and with the controller being a Raspberry Pi 3 which is using a Silicon Labs Gate driver for the MOSFET control. There are two DC power supplies, one is used as the 15 V power supply for the Gate driver and the other is used as the CC-CV charger for the cells. The oscilloscope is a Yokogawa DL850EV Scope Corder which is being used to capture the cell voltage waveforms, pack voltage, pack current, and balancing current. The CC load being used is a Chroma DC Electronic Load 63205A-1200-200.

4.1.1 Li-ion Cells

The two sets of data to be extracted for this work is the increase in useable capacity that can be achieved by using a BMS that has active discharge balance as compared to a standard BMS which is only capable of balancing the cells while charging. This data will come from two perspectives which are new cells with only a few cycles and also aged cells. The new cells are the LG Chem HG2 cells which have a nominal voltage rating of 3.6 V and capacity of 3.0 Ah. These cells are very new with only approximately 10 cycles conducted before the testing results were taken. The important specifications are listed in Table 3 and the cells can be seen in Figure 4.1.1.

Chemistry	$Li[NiMnCo]O_2$ (H-NMC) - Cathode Graphite + SiO - Anode
Nominal Voltage (V)	3.60
Std. Charging (A)	1.25
Fast Charge (A)	4.0
Nominal Capacity at 0.2C (Ah)	3.0
Maximum Continuous Discharge Current (A)	20
Capacity @ 20A, 2.8V cut-off (Ah)	2.60
Internal Resistance (mΩ)	24 - 26

Table 3: LG HG2 Cell Specifications

Figure 4.1.1: LG HG2 Test Cells

The aged cells to be used are Panasonic NCR18650 cells removed from a Lenovo laptop battery. These cells are not as power dense as the LG HG2 cells but do provide a good platform for testing 6 series that have been aged in one battery pack. These cells have a nominal voltage of 3.6 V and capacity of 2.70 Ah [63]. The important specifications are listed in Table 4 and the cells can be seen in Figure 4.1.2.

Nominal Voltage (V)	3.60
Std. Charging (A)	1.925
Maximum Continuous Discharge Current (A)	5.50
Rated Capacity (Ah)	2.7
Capacity @ 5.5A (Ah)	2.90

Table 4: Panasonic NCR18650 Cell Specifications

Figure 4.1.2: Panasonic NCR18650 Test Cells

With these cells a comparison of useable capacity increase when new can be differentiated from a set of aged cells. Even with the difference in both capacity and maximum discharge current, the standard that they are at the maximum discharge rate can be a platform for comparison.

4.1.2 18650 Cylindrical Cell Holder

The cell holder to be used must be capable of high discharge currents and should include features for secure and low resistance cell terminal connections. What was used to make the holder was a sheet of plexiglass that was folded on the sides to make a tray style base for the holder. The cell holders are standard low current cell holders, but the tin contacts were removed, and holes were drilled then threaded in place to allow a bolt to clamp the cell terminals. The bolt used is a brass threaded rod with a flat cut in, so a flat head screwdriver can be used to tighten the bolts. Aluminum nuts on the threaded rod are then used to clamp ring terminals which connect the cells

in series and also provide a high current balancing ring terminal to be added. The threaded rod heads also fit into hols in the plexiglass base to align and support the bolts. Copper flat bar then has the main conducting wire soldered to it as well as small voltage sense wires to be used by the BMS. There are also 4mm Banana Jacks for the high current balance ports and a small bread board for the sense wires so many voltage sensing probes can be used at once. It is critical that the cell holder has low resistance contacts because any voltage drop across the contacts can skew the voltage readings as the readings are in the mV range. The 18650 Cylindrical Cell Holder can be seen in Figure 4.1.3.

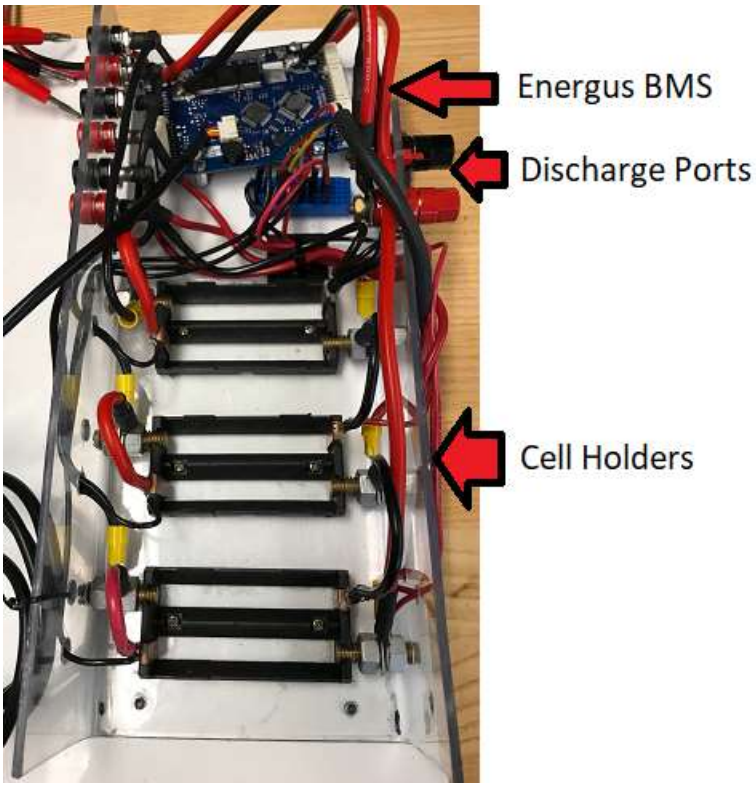

Figure 4.1.2: Cylindrical Cell Holder

4.1.3 Standard BMS

The standard BMS is an Energus Tiny s516-30A. This BMS is capable of monitoring the individual cell voltages, pack voltage, pack current, cell temperatures, and determining the SOC based on simple coulomb counting. It is capable of monitoring between 4-16 series cells and disconnecting the cells while charging and discharging in order to protect the cells. The maximum

continuous current capability is 30A with 60A peak capability for short bursts. This BMS uses passive cell balancing that is capable of 150mA balancing current. This means the BMS can only balance the cells while charging. This BMS is also used by the active BMS for voltage and current sensing as the Raspberry Pi 3 controller does not have ADC's for voltage sensing. The Energus Tiny BMS can be seen in Figure 4.1.3.

4.1.4 Active Balancing BMS

The active balancing BMS consists of four main parts in order to function. The first is the cuk converter as designed and simulated in Section 3.3. The MOSFET and diode used are both high speed and high-power devices. The MOSFET is an N-Channel Fairchild FDP8447L. The diode is a STMicroelectronics STPS20M60 Schottky Diode. This can be seen in Figure 4.1.4.

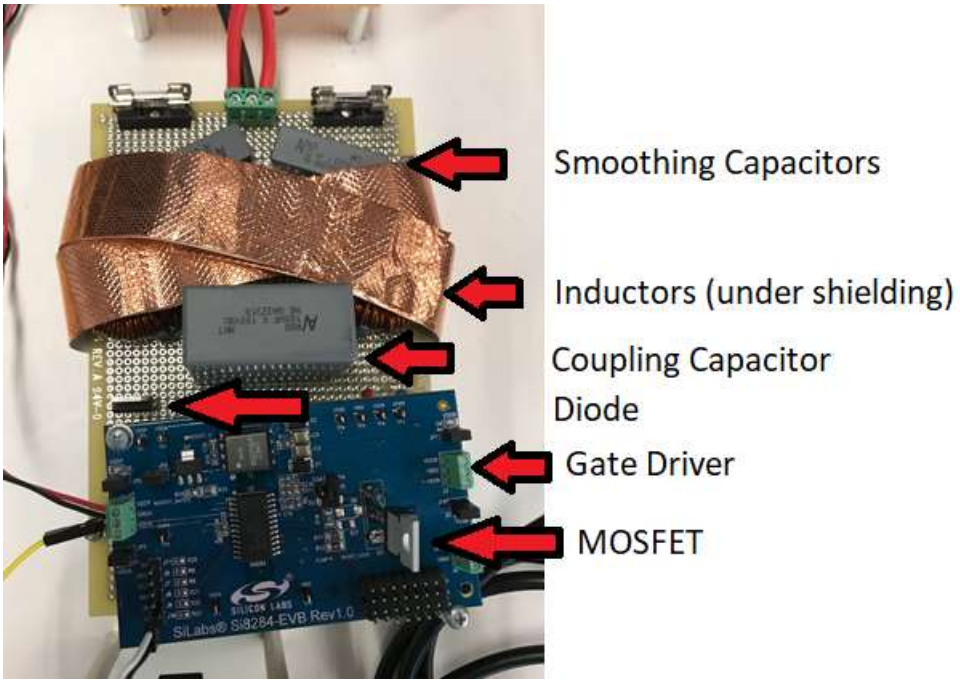

Figure 3.1.4: Cuk Converter with Si8284 Gate Driver

The gate driver for the MOSFET is a Silicon Labs Si8284 Isolated Gate Driver Evaluation kit which has the MOSFET mounted directly onto it and the connecting wires beneath the board. This Si8284 Gate Driver board requires a 15V power supply which is supplied by the Tenma 72-8695A DC Power Supply. The final parts of the active balancing BMS are the microcontroller/computer used for controlling the converter. The microcontroller which has the

control code and provides the control capability over the switch is the Raspberry Pi 3 as seen in Figure 4.1.5.

Figure 4.1.5: Raspberry Pi 3 Microcontroller

This Raspberry Pi 3 has been programmed with a user interface for simple programming using python. The Raspberry Pi is not capable of reading analog voltages so a USB to serial interface is used for the Raspberry Pi to read registers on the Energus Tiny BMS which is always monitoring the cells. This allows the Raspberry Pi to provide active discharge balancing control while not impeding the discharge cycle of the cells. The voltage readings of the imbalanced cells are then used to generate low power PWM which is sent to the Gate Driver to be amplified for proper MOSFET control.

4.1.5 DC Power Supplies

There are two DC power supplies used in these tests where one is used for cell charging when a charger is required and the other is used as a 15V supply for the Gate Driver while also supplying 12V for cooling fans used to keep the cells cool. The charging power supply is a Rigol DP832A and the 15V/12V power supply is a Tenma 72-8695A.

4.1.6 Data Recording Oscilloscope

The oscilloscope used to record data is a Yokogawa DL850EV Scope Corder. This oscilloscope is capable of 16 channels and HD data recording. The scope will have channels 1 – 6 used for reading the voltages of the 6 series cells. Channel 9 is used to record the pack current, channel 10 is used for the pack voltage and Channel 11 is used for the balancing current on the input of the cuk converter. The oscilloscope is set for 5 samples per second and after a data recording the data is saved to a USB in an Excel file generated by the oscilloscope.

4.2 Useable Capacity with Standard Balancing of Cells

The testing to determine the useable capacity of the cells with standard balancing will use only the passive balancing while charging that the Energus BMS supplies. This BMS is set to balance the cells within a 15mV band and employs early balancing, meaning a voltage set as low as 3.7 V at which the balancing can begin. This function is useful for cells that have large capacity and resistance deviations as the maximum balancing current is 150mA. Employing balancing only in the CV region with a 150mA balancing current may not be sufficient to balance the cells properly or may produce too much heat on a few resistors on the BMS board. The cells are all charged to 4.2V and have a cut-off current of 100 mA at which they are considered 100% charged.

4.2.1 Aged Panasonic NCR18650 Cells

The aged cells used are Panasonic NCR18650 cells as outlined in 4.1.1. The cells are fully charged as previously outlined and settled to room temperature before the discharge test. The discharge of the cells is a CC discharge set at 5.5A which is the maximum continuous current discharge on the datasheet of these cells. The cells are discharged to the point at which all cells have reached 2.8V. This allows a clear demonstration of the point at which all the cells pass the voltage cut-off of 3.0V. The series cell voltages during the discharge test can be seen in Figure 4.2.1. In this figure the x-axis ticks are in 50 second increments.

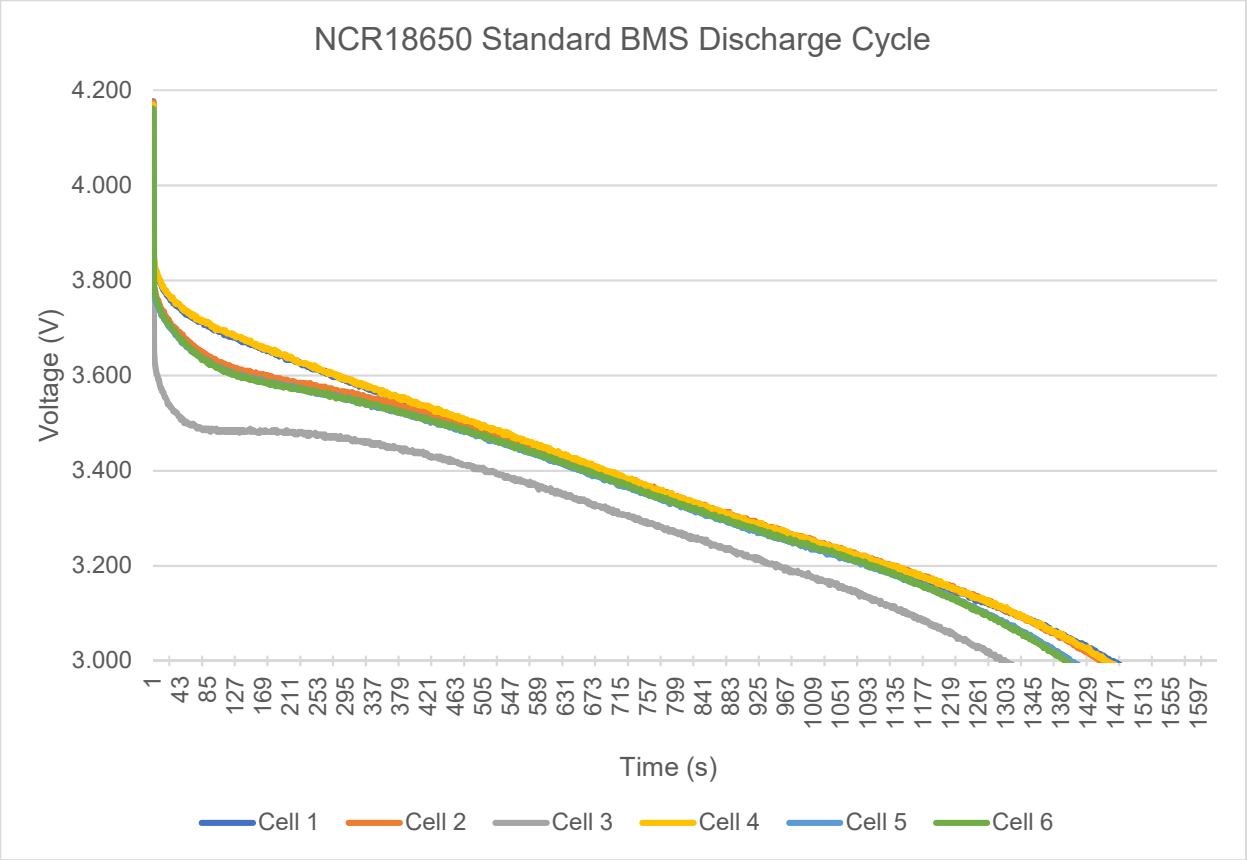

Figure 4.2.1: NCR18650 Standard BMS Discharge Cycle Graph

It can be seen that in the set of 6 series cells there is one outlier that is has a higher internal resistance than the others. The stronger cells had approximately 72 mΩ of internal resistance and the weakest cell has approximately 127 mΩ of internal resistance. There are three cells that are close together, that are close to what is the average internal resistance of the pack then there are two cells with a smaller internal resistance than the other cells. The stronger cells reached the 3.0 V cut-off in approximately 1454 seconds (24 mins, 14 seconds) and the weakest cell reached the cut-off in 1298 seconds (21 mins, 38 seconds). The end of the discharge cycle can be seen in Figure 4.2.2. In this figure the x-axis ticks are in 50 second increments.

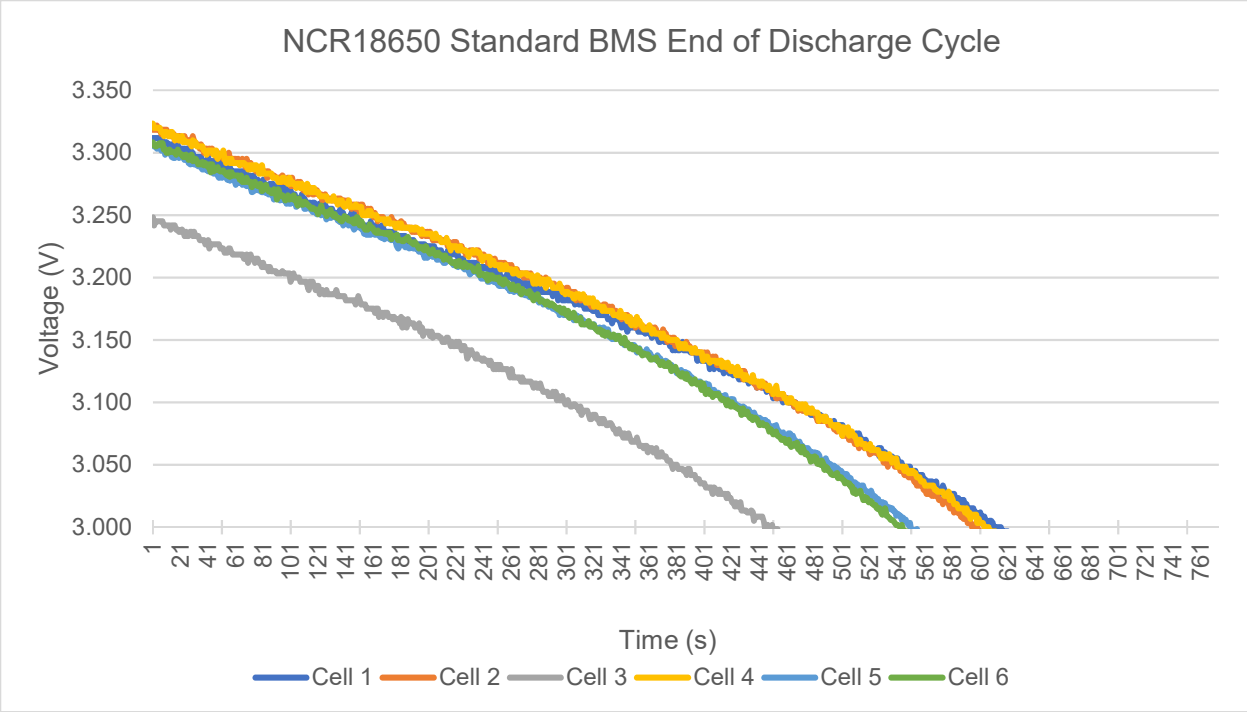

Figure 4.2.2: NCR18650 Standard BMS End of Discharge Cycle Graph

The difference in time between the average cells and the weaker cell is approximately 100 seconds which relates to 153 mAh. The difference between the weak cell and the strongest cells is 160 seconds which relates to 244 mAh. The point midway between the weakest cell and strongest cell is 80 seconds and 122 mAh. With discharge balancing this can be an approximated gain in useable capacity when utilizing a standard voltage cut-off. The approximated gain is also 6.16% by comparing the cut-off time of 1298 seconds without balancing to the 1378 seconds with balancing. The values of total capacity drained from the cells to a 3.0V cut-off at the maximum rated current can be found in Table 5.

Cell Specifications	Discharged Capacity (Ah)	SOH (%)
0-Cycle Capacity	2.550	100
Weakest cell	1.983	77.76
Average cells	2.131	83.57
Strongest cells	2.221	87.10

Table 5: NCR18650 Discharged Capacity

These aged cells were considered to be at EOL, but it can be seen that the limiting factor to the SOH is the weakest cell meanwhile the average of the pack is not yet at EOL.

4.2.2 New LG Chem INR18650HG2 Cells

The new cells used are LG HG2 cells as outlined in 4.1.1. The cells are fully charged as previously outlined and settled to room temperature before the discharge test. The discharge of the cells is a CC discharge set at 20.0A which is the maximum continuous current discharge on the datasheet of these cells. The cells are discharged to the point at which all cells have reached 2.7V. This allows a clear demonstration of the point at which all the cells pass the voltage cut-off of 2.8V. The cut-off of 2.8V was chosen because at 20A the point at which the cells begin to go into the non—linear end of SOC region begins near that point. At a 3.0V cut-off, a significant portion of the capacity is not utilized and realistic for the actual implementation for high output cells. The series cell voltages can be seen in Figure 4.2.3. In this figure the x-axis ticks are in 20 second increments.

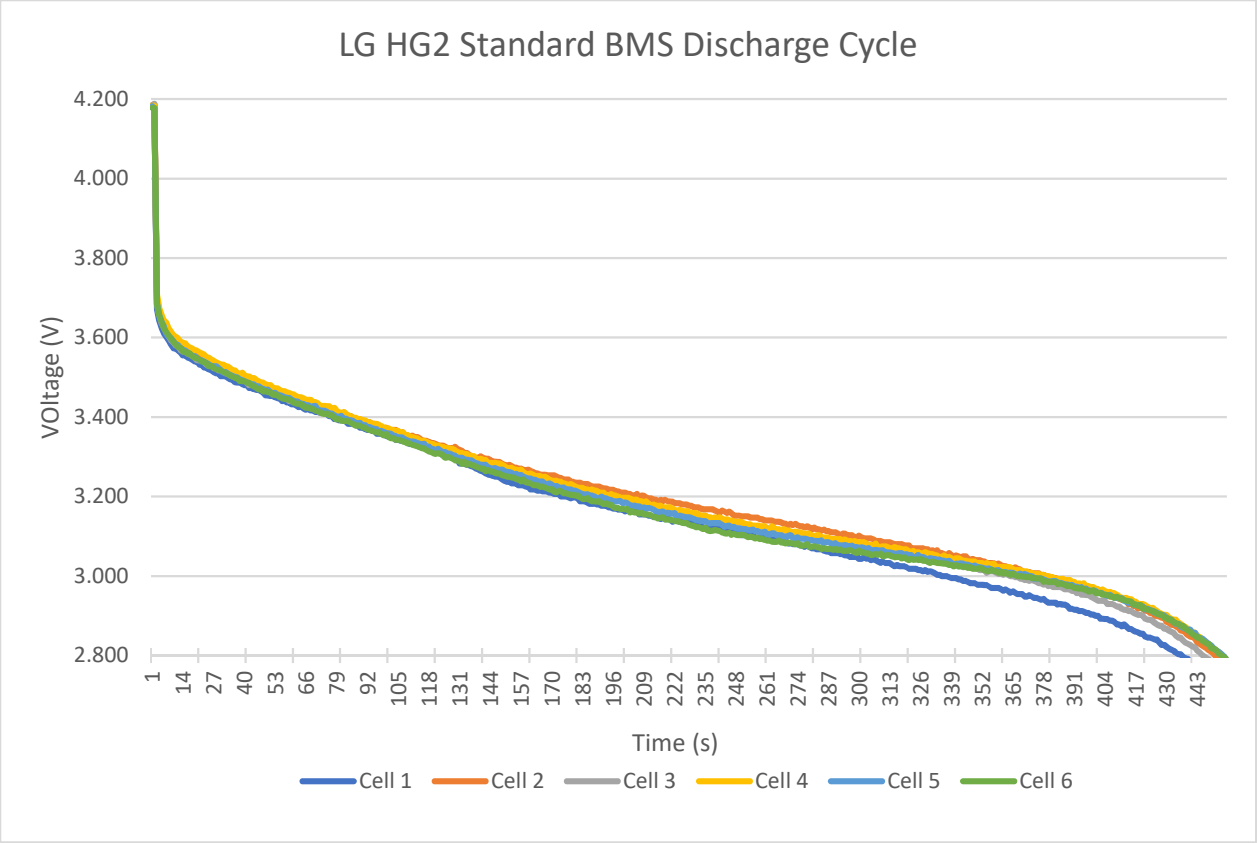

Figure 4.2.3: LG HG2 Standard BMS Discharge Cycle Graph

It can be seen that in the set of 6 series cells there is one outlier that is has a higher internal resistance than the others. It is not a very large difference as all the cells have approximately 30 mΩ of internal resistance but at 20A a small difference can appear by the end of the cycle. There are three cells that are close together that are close to what is the average internal resistance of the pack then there are two cells with a smaller internal resistance than the other cells. The stronger cells reached the 2.8 V cut-off in approximately 456 seconds (7 mins, 36 seconds) and the weakest cell reached the cut-off in 438 seconds (7 mins, 18 seconds). The end of the discharge cycle can be seen in Figure 4.2.4. In this figure the x-axis ticks are in 5 second increments.

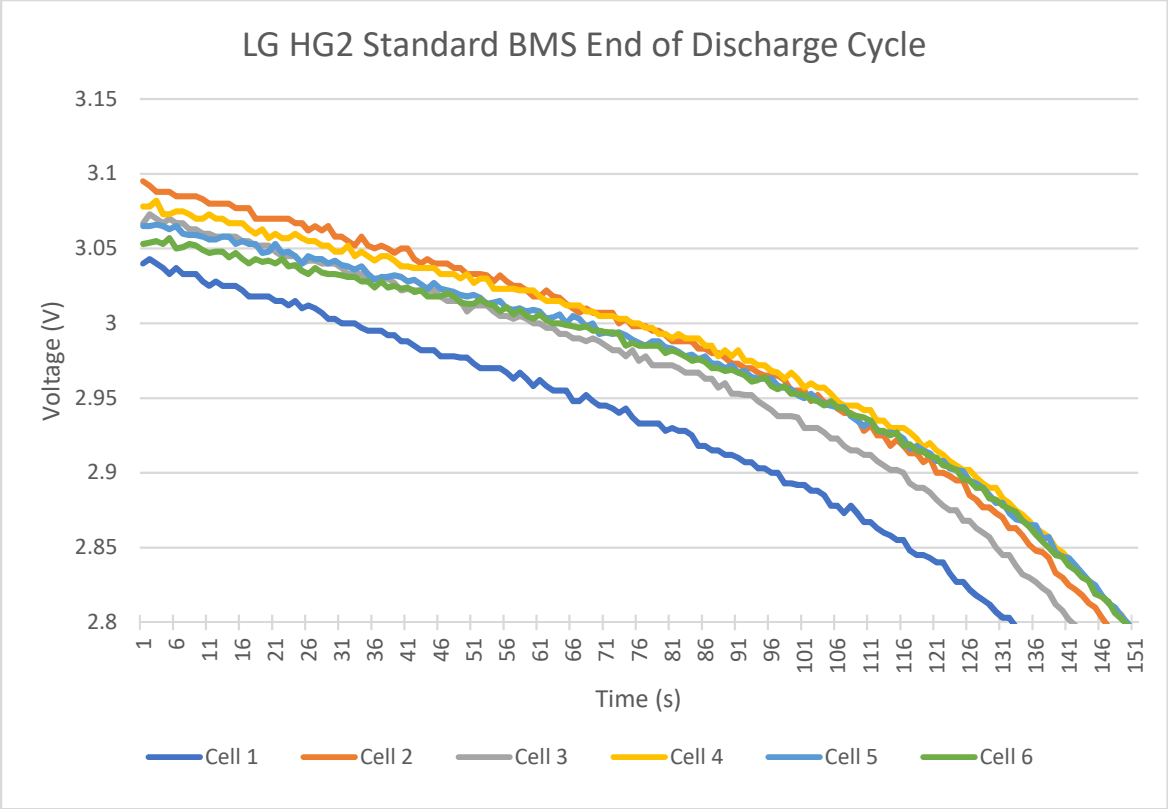

Figure 4.2.4: LG HG2 Standard BMS End of Discharge Cycle Graph

The difference in time between the stronger cells and the weaker cell is approximately 18 seconds which relates to 100 mAh at 20A. The point midway between the weakest cell and strongest cell is 9 seconds and 50 mAh. With discharge balancing this can be an approximated gain in useable capacity when utilizing a standard voltage cut-off. The approximated gain is also 2.05% by comparing the cut-off time of 438 seconds without balancing to the 447 seconds with balancing. The values of total capacity drained from the cells to a 2.8V cut-off at the maximum rated current can be found in Table 6. Overall, these cells were very close to in SOH with 4% difference in capacity.

Cell Specification	Discharged Capacity (Ah)	SOH (%)
0-Cycle Capacity	2.600	100
Weakest Cell	2.533	97.42
Stronger Cells	2.433	93.58

Table 6: LG HG2 Discharged Capacity

4.3 Useable Capacity with Discharge Balancing of Cells

The testing to determine the useable increase in capacity of the cells with the discharge balancing is the exact same as the standard BMS testing except for the addition of discharge balancing below 3.1V on the strongest and weakest cells. The same Energus BMS carries out the charge balancing to a tolerance band of 15mV between cells with a charging cut-off current of 100mA the same as the standard BMS testing. The cut-off voltages are the same for all the tests as compared to the standard BMS testing.

4.3.1 Aged Panasonic NCR18650 Cells

The cells are fully charged as previously outlined and settled to room temperature before the discharge test. The discharge of the cells is a CC discharge set at 5.5A the same as the previous test with the aged cells. The cells are discharged to the point at which all cells have reached 2.8V. This allows a clear demonstration of the point at which all the cells pass the voltage cut-off. The active discharge balancer is engaged when the weaker cell has reached 3.1V as outlined in the control strategy in Section 3.5. The cell orientation is the same as the standard BMS test as the tests were done back to back with the converter input being connected to cell 4 and the output to cell 3. The series cell voltages during the discharge test can be seen in Figure 4.3.1. In Figure 4.3.1, the x-axis ticks are in 50 second increments. In Figure 4.3.2, the x-axis ticks are in 20 second increments.

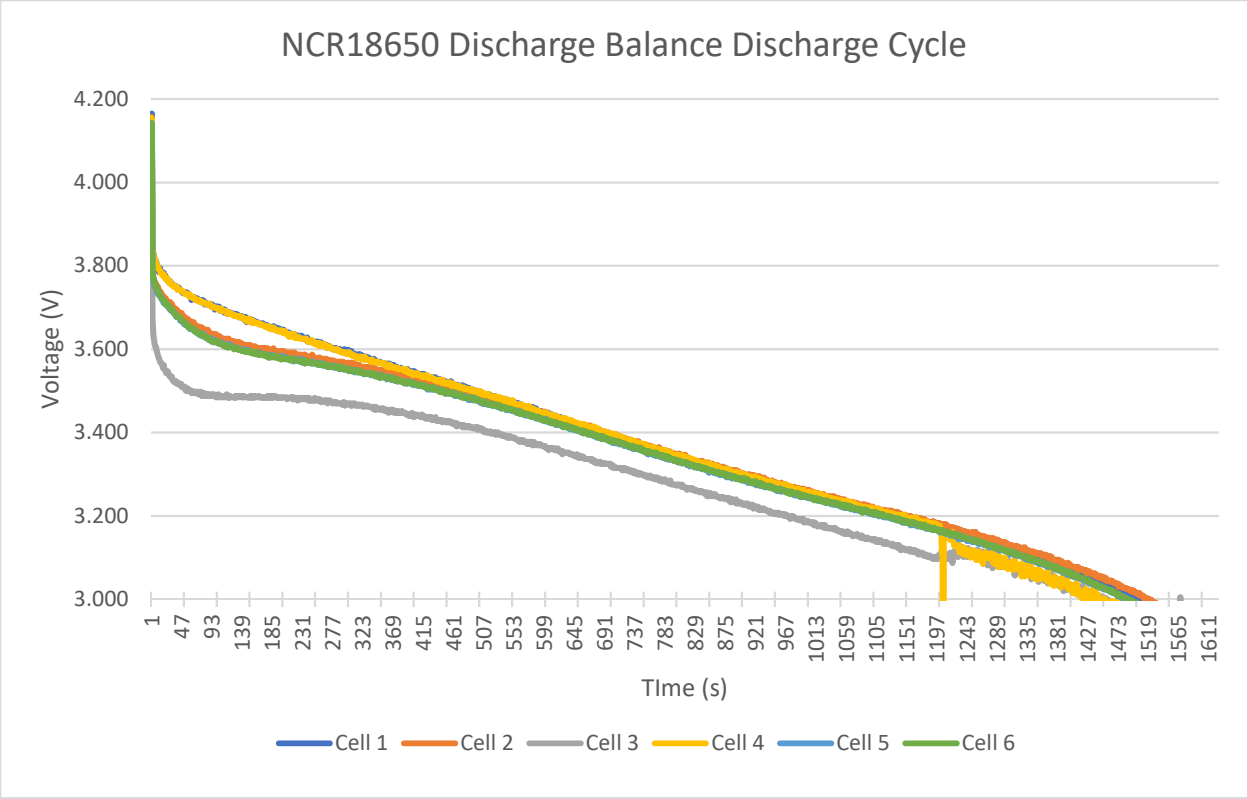

Figure 4.3.1: NCR18650 Discharge Balance Discharge Cycle Graph

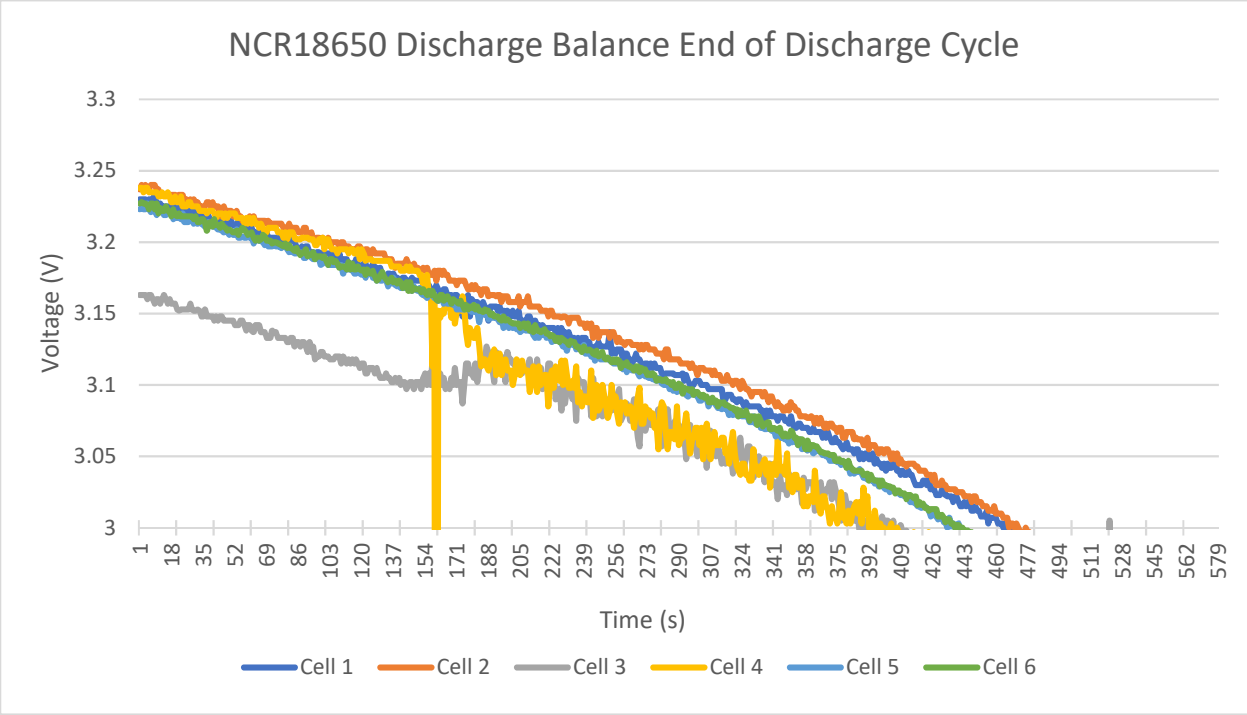

Figure 4.3.2: NCR18650 Discharge Balance End of Discharge Cycle Graph

As seen in Figure 4.3.1 and 4.3.2, the point at which the weakest cell reaches the 3.0V cut-off is now extended and the useable capacity remaining in the stronger cell is being utilized. The capacity discharged from all the cells in this test is different than the standard BMS test in Section 4.2.1. This could be because of different room temperatures or different cell temperatures during the test. Using the same curve pattern, the end point can be used to estimate the increase in useable capacity from these aged cells. Cell 2 was the strongest cell in this test and reached the cut-off at 1521 seconds (25 mins, 21 seconds), Cell 6 was taken as the pack average which reached the cut-off at 1491 seconds (24 mins, 51 seconds), and Cell 3 and 4 were first to reach the cut-off at 1458 seconds (24 mins, 18 seconds). The approximated point at which the weakest cell would have reached the cut-off if looking at the time capacity difference from the standard BMS test in Section 4.2.1 is 1361 seconds (22 mins, 41 seconds). The values of total capacity drained from the cells to a 3.0V cut-off at the maximum rated current can be found in Table 7.

Cell Specifications	Discharged Capacity (Ah)
First cells to 3.0V	2.228
Average cells	2.280
Strongest cells	2.324
Approximated capacity without discharge balancing	2.079

Table 7: NCR18650 Discharge Capacity with Discharge Balancing

Therefore, the increase in useable capacity with discharge balancing at a cut-off of 3.0V is 149 mAh and this correlates to an increase of 7.2% in useable capacity from the aged cells. Looking at the other important characteristics of the active balancer, the voltage ripple seen on both cells being balanced is less than 30mV which is within the 50mV maximum the converter was designed for. The converter and control algorithm was also able to keep the cells within 10mV of each other approximately when dismissing the voltage ripple seen. The balancing current as in Figure 4.3.3, is not very smooth with an average of 600mA ripple. This is not entirely due to the controller but rather the PWM generating capability of the Raspberry Pi 3. This controller is not designed to drive PWM at the 37.5 kHz frequency which it was driving for the test. This PWM was jittery and not smooth, the duty cycle seen also was not what the controller was displaying.

The jitter and stutter from the PWM being generated by the Raspberry PI was also audible from the inductors movement during the test. The duty cycle was around the 70% region according to the controller but when measured was actually 55% which is close to what was simulated in Section 3.4. A large in-rush current is also seen when the converter is engaged because the controller was setup to begin the duty cycle at 50%, the current spike can also be seen as a voltage drop on Cell 4. The balancing current in Figure 4.3.3 was read at the input of the converter.

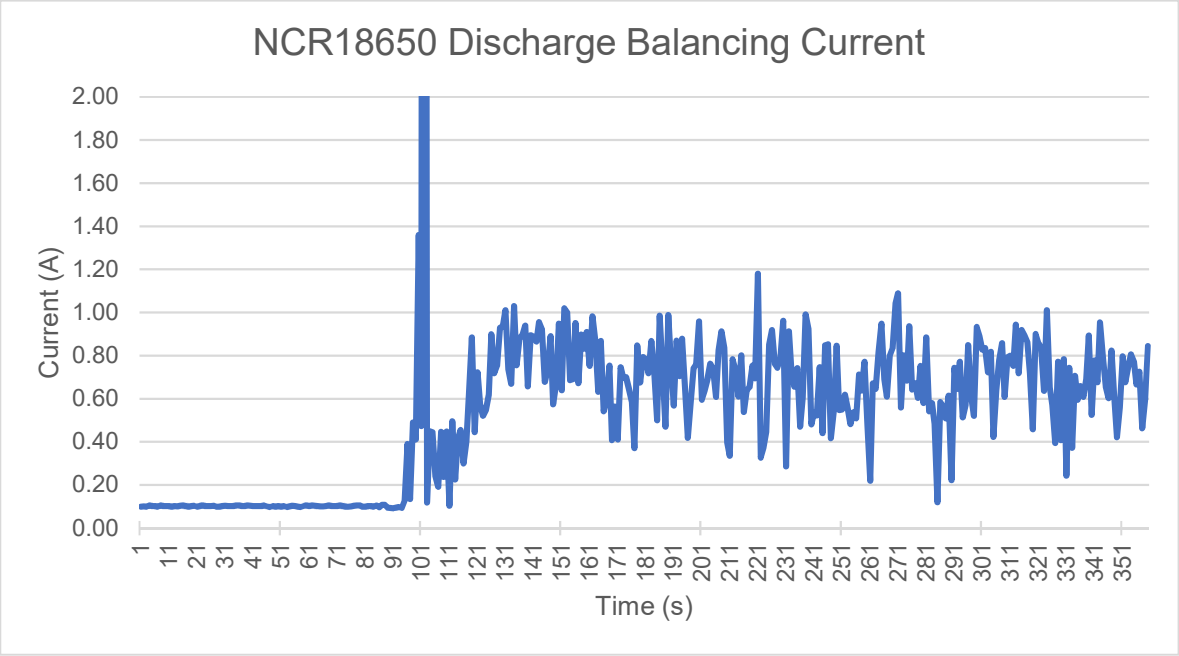

Figure 4.3.3: NCR18650 Discharge Balancing Current Graph

4.3.2 New LG Chem INR18650HG2 Cells

The cells are fully charged as previously outlined and settled to room temperature before the discharge test. The discharge of the cells is a CC discharge set at 20A the same as the previous test with the new cells. The cells are discharged to the point at which all cells have reached 2.7V. This allows a clear demonstration of the point at which all the cells pass the voltage cut-off of 2.8V. The active discharge balancer is engaged when the weaker cell has reached 3.1V as outlined in the control strategy in Section 3.5. The converter output was connected to the weaker cell in cell holder 1 and the input of the converter was connected to cell holder 2. The series cell voltages during the discharge test can be seen in Figure 4.3.4. In Figure 4.3.4, the x-axis ticks are in 20 second increments. In Figure 4.3.5, the x-axis ticks are in 5 second increments.

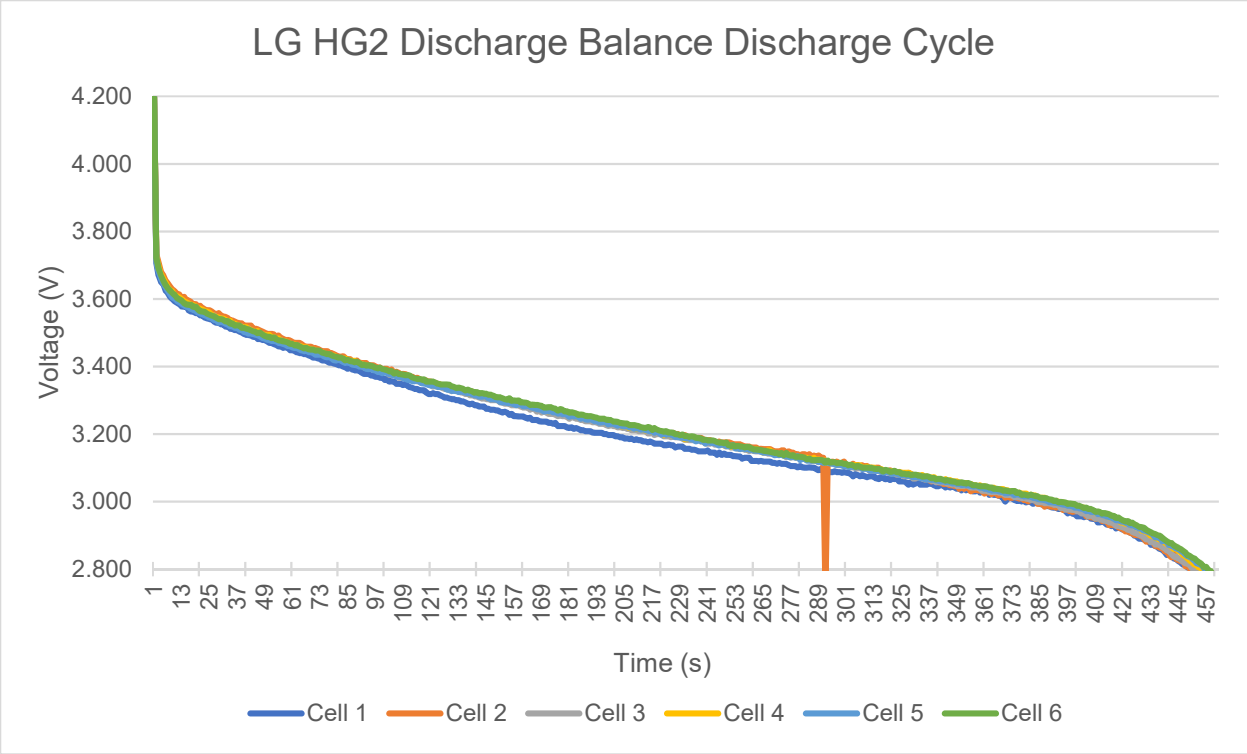

Figure 4.3.4: LG HG2 Discharge Balance Discharge Cycle Graph

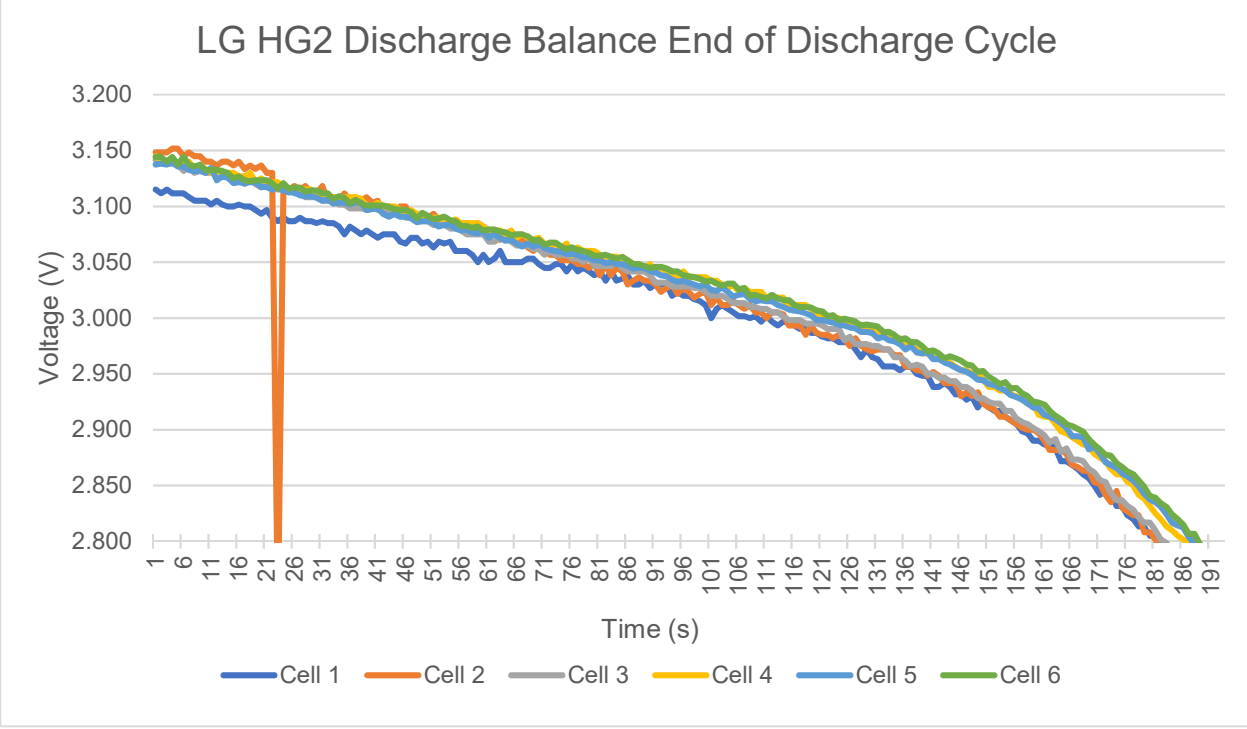

Figure 4.3.5: LG HG2 Discharge Balance End of Discharge Cycle

As seen in Figure 4.3.4 and 4.3.5, the point at which the weakest cell reaches the 2.8V cut-off is now extended and the useable capacity remaining in the stronger cell is being utilized. Cell 6 was the strongest cell in this test and reached the cut-off at 459 seconds (7 mins, 39 seconds), Cell 4 was taken as the pack average which reached the cut-off at 456 seconds (7 mins, 36 seconds), and Cell 1 and 2 were first to reach the cut-off at 452 seconds (7 mins, 32 seconds). The approximated point at which the weakest cell would have reached the cut-off if looking at the time capacity difference from the standard BMS test in Section 4.2.2 is 441 seconds (7 mins, 21 seconds). The values of total capacity drained from the cells to a 2.8V cut-off at the maximum rated current can be found in Table 8.

Cell Specifications	Discharged Capacity (Ah)
First cells to 2.8V	2.511
Average cells	2.533
Strongest cells	2.55
Approximated capacity without discharge balancing	2.450

Table 8: LG HG2 Discharge Capacity with Discharge Balancing

Therefore, the increase in useable capacity with discharge balancing at a cut-off of 2.8V is 61 mAh and this correlates to an increase of 2.49% in useable capacity from the new cells. The voltage ripple seen on both cells being balanced is less than 20mV which is within the 50mV maximum the converter was designed for. The converter and control algorithm was also able to keep the cells within 10mV of each other approximately when dismissing the voltage ripple seen. The balancing current as in Figure 4.3.6, is not very smooth with an average of 500mA ripple. This is the same result as seen and explained in Section 4.3.1. A large in-rush current is also seen when the converter is engaged because the controller was setup to begin the duty cycle at 50%, the current spike can also be seen as a voltage drop on Cell 2. The balancing current was read at the input of the converter.

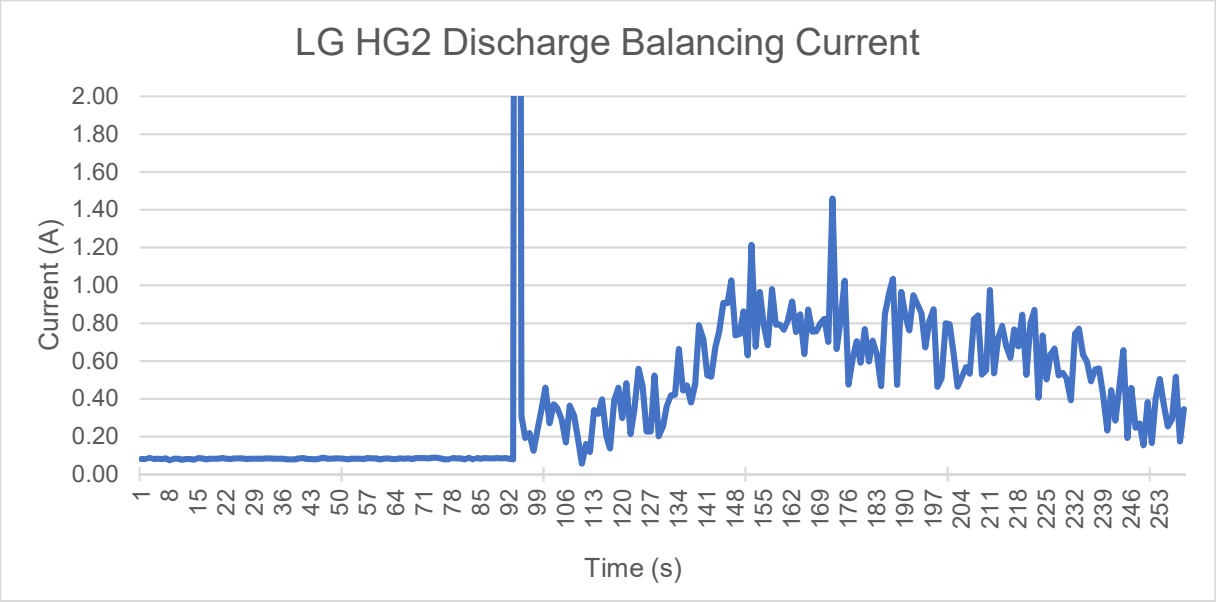

Figure 4.3.6: LG HG2 Discharge Balancing Current Graph

4.4 Summary

This chapter outlines all the test equipment, the new and aged cells to be tested, and the test procedures with the relating conditions. The cell characteristics were studied and examined during the tests and compared to new. The aged cells were seen to be at EOL while the new cells after 10 cycles had some note-able capacity loss after 10 cycles as well as one cell which was weaker than the others. The standard tests were conducted to get a baseline for the limiting factor of the useable capacity in the pack as well as the remaining useful capacity in the other cells. The active discharge balancing test was carried out with the aged cells and the new cells. It was shown that a 7.2% and 2.49% increase in useable capacity was possible with the aged and new cells respectively. This demonstrates that the discharge balancing technique is capable of increasing the useable capacity in both new and aged cells when an industry standard BMS voltage cut—off is utilized. It can also be seen that the balancing increases the useable capacity close to the average pack useable capacity irrespective of the cell age. Furthermore, for the aged cells the first cells to reach the cut-off had a useable capacity of 2.228 Ah and this would correlate to 87.3% SOH. If the cells were produced when the first NCR18650 cells were produced in 2012, then the cells would have about another 3.5 years of useable life until EOL if they had the same aging rate as their current life depicts.

Chapter 5

Conclusion and Future Work

This thesis focuses on the increase of useable capacity in Li-ion batteries for EV's with standard BMS control techniques by utilizing an active cell equalizer near the end of the discharge cycle to reduce the load on the weaker cell of a stack by utilizing remaining capacity in a stronger cell. Chapter 1 and 2 of this thesis provide the foundation for the knowledge on all aspects of the BMS as well as Li-ion characteristics. The industry standard BMS solely focuses on cost so passive cell equalizers are used and this leads to issues with charging speed, cell degradation differences in a series stack, and limits on the useable capacity from the cells. The third chapter delves deeper into the understanding and applicable solutions for balancing series cells while discharging. From the possible solutions an active cell equalizer is developed and simulated to demonstrate it is capable of balancing cells whether they are charging, discharging, or idle.

In the fourth chapter the testing equipment, new and aged cells, and hardware implementation of the active balancing BMS is outlined. The testing procedure is explained in detail to get an accurate comparison of the useable capacity from standard BMS and from a BMS that is capable of discharge balancing. It was experimentally verified that discharge balancing could improve the useable capacity of new cells by 2.49%. The useable capacity with discharge balancing on aged cells near EOL showed an increase of 7.2%.

5.1 Contribution

- A thorough study of the characteristics exhibited by Li-ion cells was studied in the first three chapters. The understanding of the characteristics, aging mechanisms, cell reactions, and implementation of Li-ion batteries is critical to the improvement of their use in EV's.
- A review was conducted on the SOC estimation techniques that are implemented into EV BMS systems or researched to be a future component of BMS. The SOC estimation that a BMS uses is critical to the was the BMS can maintain and control the cells to improve range, cell life, efficiency, and accurately approximate the SOC remaining in the cells.
- The topologies studied and also implemented on all forms BMS were reviewed in detail to understand which topology would be adequate for discharge balancing. The topologies were also compared, and their characteristics discussed to provide detail on advantages and disadvantages.
- A Cuk converter based Active Balancing BMS was designed and simulated in Chapter 3 to provide the platform of which a discharge balancing capable BMS was designed. The control algorithm was also designed for implementation with industry standard voltage cut-off cell protection.
- In Chapter 4 the testing procedure, equipment, and components to conduct testing on new and aged cells was outlined. The active balancing BMS was built and used to carry out the balancing during maximum power discharging of Li-ion cells. Discharge balancing during maximum power discharging was experimentally justified to show an improvement of 7.2% in aged cells which were near EOL and had a capacity difference of 12% between the strongest and weakest cells under testing without active discharge balancing. The discharge balancing was shown to increase the useable capacity in cells near new, with only 10 cycles, by 2.49% where the capacity difference was 4.11%.

5.2 Future Work

- The design of the converter for an active balancing BMS was designed and tested but only for a single pair of cells which were neighbouring cells. Only one converter was used to

carry out the experimental verification of discharge balancing in order to prove the scope of this thesis. The simulation, control and experimental testing of a full BMS with multiple converters to balance any two cells anywhere in the stack could prove effective for industry application. The optimization of the converter for specific applications can be determined through different cost, balancing speed, and efficiency optimization requirements.

- The venue of SOC balancing as compared to strictly instantaneous voltage balancing could prove to be a more effective way to balance cells and extend lifetime. This would require the application and verification of an advanced SOC estimation technique but would greatly improve the effectiveness and efficiency of the use of the discharge balancing technique.
- In this thesis the increase in useable capacity with discharge balancing was the only aspect that was experimentally verified for the active BMS. The research into SOH estimation techniques and the lifetime cycling of cells with this active BMS with comparisons to a standard BMS would prove the increase in battery life that is capable from discharge balancing.
- The converter was designed for discharge balancing strictly and was also only implemented for discharge balancing. The same converter can be controlled and used for charge balancing. The experimental verification of charge balancing and especially under fast charge scenarios with new and aged cells can be carried out to justify the reduction in charge time in the CV region with respect to a standard BMS with passive balancing.

Appendix A

Datasheets Graphs

LG HG2 Datasheet Graph

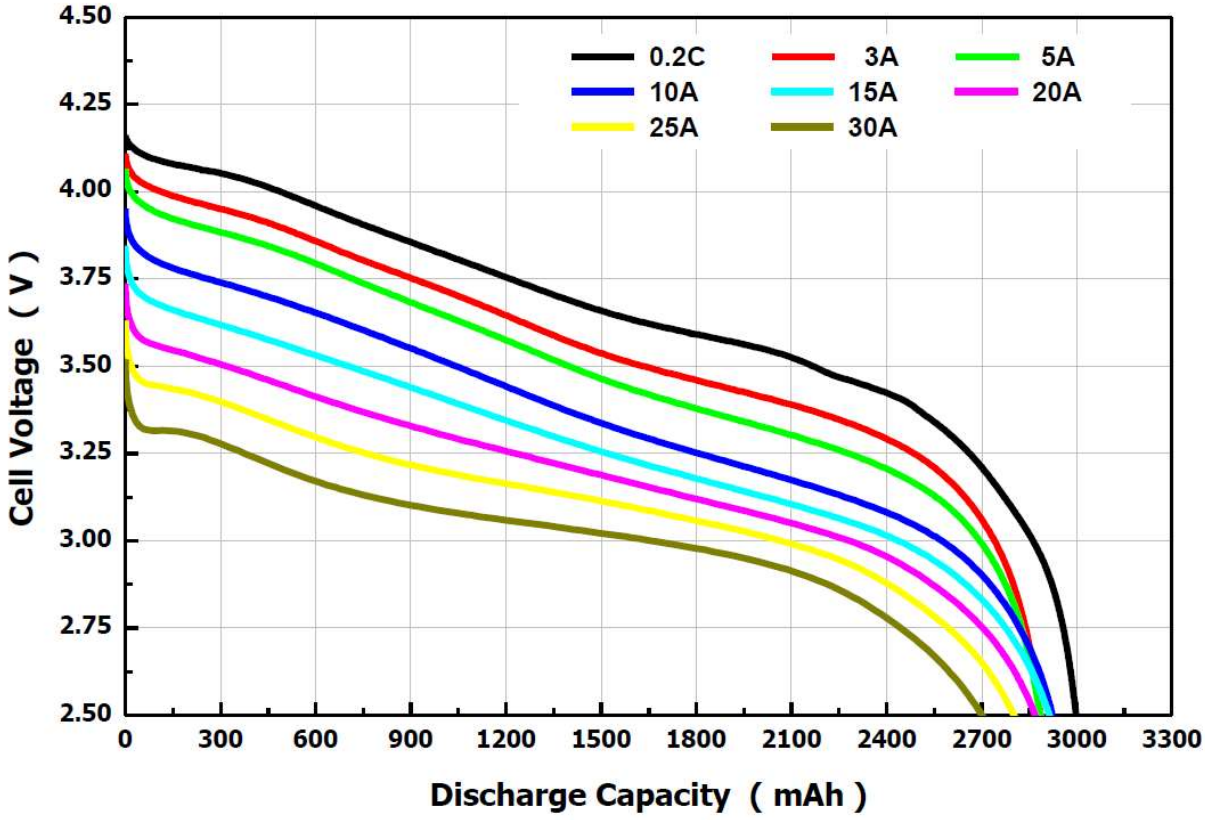

Panasonic NCR18650 Datasheet Graph

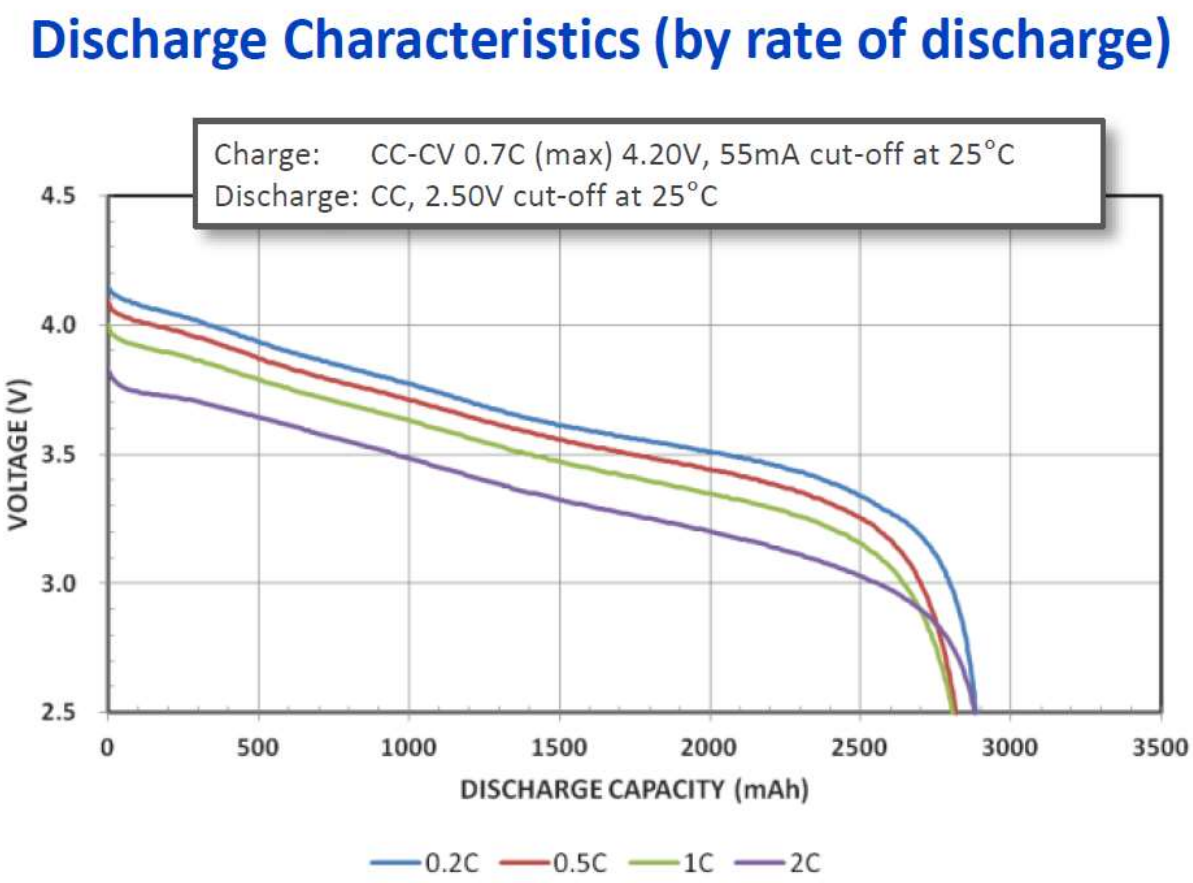

Appendix B

Single Cell Equalizer Control Flowchart

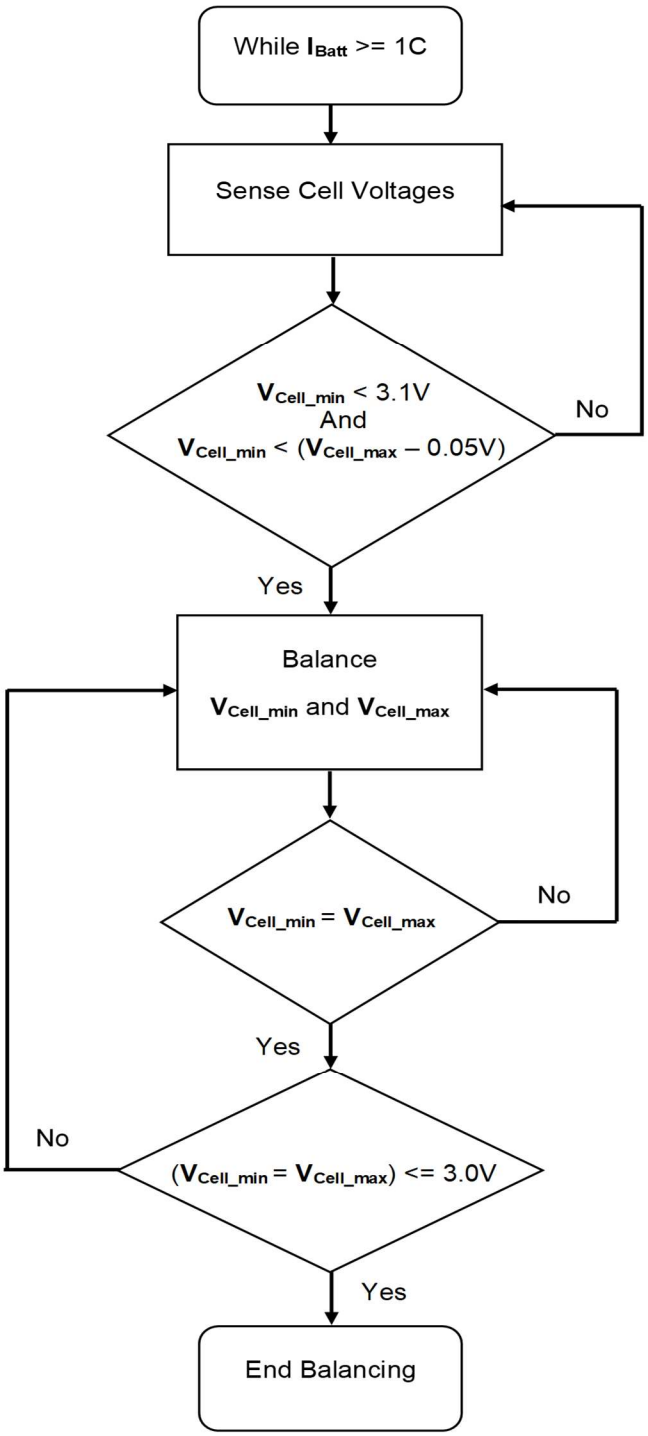

Appendix C

Python Code implemented on the Raspberry Pi

BatteryBalance.py

```
import sys
import math
sys.path.append('/usr/local/lib/python2.7/dist-packages')        #add the directory of minimalmodbus library
import minimalmodbus                    #import library for minimal modbus to read data from BMS registers
import time

minimalmodbus.BAUDRATE = 115200                                  #set baudrate to 115200 bits/second
#initializing the BMS, port name changes, to determine name open pi command terminal, write dmesg, and look for cp210x USB port
instrument = minimalmodbus.Instrument('/dev/ttyUSB0', 170) # port name, slave address (in decimal)

#import and setup GPIO
import RPi.GPIO as GPIO
GPIO.setmode(GPIO.BCM)
GPIO.setwarnings(False)
GPIO.setup(18,GPIO.OUT)                                          #set pin 18 as output
p = GPIO.PWM(18,50)
p.ChangeFrequency(37500)
dischargeState = False

def discharge(check = False):                                    #This is the function to test the state of discharge
        if current > 2.75:
                print("Discharging")
                return True
        else:
                print("Not Discharging")
                return False

def updateValues():
   ## Read the register value (PV = ProcessValue) ##
   ## FORMAT: Registernumber, number of decimals## Read the register value (PV = ProcessValue) ##
   cell_1 = instrument.read_register(15, 4)
   cell_2 = instrument.read_register(14, 4)
   cell_3 = instrument.read_register(13, 4)
   cell_4 = instrument.read_register(12, 4)
   cell_5 = instrument.read_register(11, 4)
   cell_6 = instrument.read_register(10, 4)
   current = instrument.read_register(38, 3)
```

```
    maxV = instrument.read_register(39, 4)
    minV = instrument.read_register(40, 4)

def main():
    cellDifference = True
    duty = 50
    maxV = instrument.read_register(39, 4)                  # Registernumber, number of decimals
    minV = instrument.read_register(40, 4)                  # Registernumber, number of
decimalsupdateValues()
    p.start(0)
    while cellDifference == True and discharge(dischargeState) == True:
        while (minV < 3.10 and minV < (maxV - 0.05)):
            maxV = instrument.read_register(39, 4) # Registernumber, number of decimals
            minV = instrument.read_register(40, 4) # Registernumber, number of decimalsupdateValues()
            print("Balancing")
            print("The maximum cell: ", maxV, "V")
            print("The minimum cell: ", minV, "V")
            print("Duty Cycle: ", duty)
            duty = duty + 0.2*(maxV - minV)
            p.ChangeDutyCycle(duty)

            if duty >= 90:
                duty = 90
                p.ChangeDutyCycle(duty)
                print("Maximum Duty Cycle Reached")

            elif duty <= 30:
                duty = 30
                p.ChangeDutyCycle(30)
                print("Minimum Duty Cycle Reached")

            elif ((minV <= (maxV + 0.01) and minV >= maxV) or (minV >= (maxV - 0.01) and minV <=
maxV)) and maxV <= 2.80:
                print("Max and Min cells are balanced")
                print("Cell Difference: ", maxV - minV, " V")
                duty = 0
                cellDifference = False
                p.ChangeDutyCycle(duty)
                p.stop()
                print(duty)
main()
```

Bibliography

[1] C. Sulzberger. (2004, June 14). An early road warrior: electric vehicles in the early years of the automobile. *IEEE Power and Energy Magazine*. [Online]. pp. 66-71. Available: https://ieeexplore.ieee.org/document/1293606/

[2] K. Nesbitt and J. Davies, "From the Top of the Organization to the Bottom Line: Understanding the Fleet Market for Plug-in Electric Vehicles," presented at the Electric Vehicle Symp. And Exhibition, Barcelona, Spain, 2013.

[3] F. Richter. (2017, Jan.). Can Falling Battery Prices Push Electric Cars?. Electric Mobility. [Online]. Available: https://www.statista.com/chart/7713/electric-car-battery-prices/

[4] C. Haoxiang et al., "Information flow and its fusion of EV's intelligent integrated station," presented at the China Int. Conf. on Electricity Distribution, Shenzhen, China, 2014.

[5] S.D Rao Vadlamudi.et al., "Hybrid Energy Storage Power Allocation and Motor Control for Electric Forklifts," presented at the Asian Conf. on Energy, Power and Transportation Electrification, Singapore, 2016.

[6] A.O. Al-Jazaeri et al., "Fuzzy Logic Control for energy saving in Autonomous Electric Vehicles," presented at IEEE Electric Vehicle Conf., Florence, Italy, 2014.

[7] S.R. Wright, "Overcoming the high cost of EV batteries," presented at the Battery Conf. on Application and Advances, Long Beach, CA, 1995.

[8] R.A. Hanifah et al., "Electric Vehicle Battery Modelling and Performance Comparison in Relation to Range Anxiety," presented at IEEE Int. Symp. On Robotics and Intelligent Sensors, Langkawi, Malaysia, 2015.

[9] J. Qian et al. (2015, Feb.). High rate and stable cycling of lithium metal anode. *Nature Communications*[Online]. *6(6362)*, doi: 10.1038/ncomms7362. Available: https://www.nature.com/articles/ncomms7362.pdf

[10] T. Horiba, "Lithium-ion battery systems," *Proc. IEEE* vol. 102, pp. 939-950, June 2014.

[11] Otto A. et al. (2012) Battery Management Network for Fully Electrical Vehicles Featuring Smart Systems at Cell and Pack Level. In: Meyer G. (eds) Advanced Microsystems for Automotive Applications 2012. Springer, Berlin, Heidelberg.

[12] L.H. Saw et al., “Thermal Management of Lithium-ion Battery Pack with Liquid Cooling,” presented at Thermal Measurement, Modeling and Management Symp., San Jose, CA, 2015.

[13] Miguel D. Beirão, Maria do Rosário A. Calado, José A.N. Pombo, Sílvio J.P.S. Mariano (2016) Balancing management system for improving Li-ion batteries capacity usage and lifespan. Paper presented at the 16th IEEE International Conference on Environment and Electrical Engineering (EEEIC), Florence, Italy, 7-10 June 2016.

[14] CCsar Pascual and Philip T. Krein (1997) Switched capacitor system for automatic series battery equalization. Paper presented at 12th IEEE Applied Power Electronics Conference and Exposition (APEC), Atlanta, GA, 27-27 Feb. 1997.

[15] K. Nishijima, H. Sakamoto and K. Harada (2000) A PWM Controlled Simple and High-Performance Battery Balancing System. Paper presented at 31st IEEE Power Electronics Specialists Conference (PESC), Galway, Ireland, 23-23 June 2000

[16] Andrew C. Baughman and Mehdi Ferdowsi (2008) Double-Tiered Switched-Capacitor Battery Charge Equalization Technique. IEEE Transactions on Industrial Electronics 55(6):2277-2285.doi: 10.1109/TIE.2008.918401

[17] Sang-Hyun Park, Tae-Sung Kim, Jin-Sik Park, Gun-Woo Moon and Myung-Joong Yoon (2009) A New Buck-boost Type Battery Equalizer. Paper presented at 24th IEEE Applied Power Electronics Conference and Exposition (APEC), Washington, DC, 15-19 Feb. 2009.

[18] Pablo A. Cassani, Sheldon S. Williamson (2010) Design, Testing, and Validation of a Simplified Control Scheme for a Novel Plug-In Hybrid Electric Vehicle Battery Cell Equalizer. IEEE Transactions on Industrial Electronics 57:3956-3962.doi: 10.1109/TIE.2010.2050750

[19] Masatoshi Uno, and Koji Tanaka (2011) Single-Switch Cell Voltage Equalizer Using Multistacked Buck-Boost Converters Operating in Discontinuous Conduction Mode for Series-Connected Energy Storage Cells. IEEE Transactions on Vehicular Technology 60(8):3635-3645.doi: 10.1109/TVT.2011.2165229

[20] Yuang-Shung Lee and Guo-Tian Cheng (2006) Quasi-Resonant Zero-Current-Switching Bidirectional Converter for Battery Equalization Applications. IEEE Transactions on Power Electronics 21(5):1213-1224.doi: 10.1109/TPEL.2006.880349

[21] P. Barrade (2002) Series connection of supercapacitors: comparative study of solutions for the active equalization of the voltages. Paper presented at Electrimacs 7th International Conference on Modeling and Simulation of Electric Machines, Converters and Systems, Montréal, QC, 18-21 August 2002.

[22] Sang-Hyun Park, Ki-Bum Park, Hyoung-Suk Kim, Gun-Woo Moon, and Myung-Joong Youn (2012) Single-Magnetic Cell-to-Cell Charge Equalization Converter With Reduced Number of Transformer Windings. IEEE Transactions on Power Electronics 27(6):2900-2911.doi: 10.1109/TPEL.2011.2178040

[23] A. I. Stan et al., “Lithium Ion Battery Chemistries from Renewable Energy Storage to Automotive and Back-up Power Applications - An Overview,” presented at Int. Conf. on Optimization of Electrical and Electronic Equipment, Bran, Romania, July 2014.

[24] J. Leuchter and P. Bauer, “Capacity of Power-Batteries versus Temperature,” presented at European Conf. on Power Electronics and Applications, Geneva, Switzerland, Oct. 2015.

[25] F. Leng et al. (2015, Aug.). Effect of Temperature on the Aging rate of Li Ion Battery Operating above Room Temperature. Scientific Reports[Online]. 5(12967), doi: 10.1038/srep12967. Available: https://www.nature.com/articles/srep12967.pdf

[26] E. Martinez-Laserna et al., “Evaluation of Lithium-ion Battery Second Life Performance and Degradation,” presented at IEEE Energy Conversion Congr. And Expo., Milwaukee, WI, 18-22 Sept., 2016.

[27] J. Remmlinger et al. (2010, Aug.). State-of-health monitoring of lithium-ion batteries in electric vehicles by on-board internal resistance estimation. *Journal of Power Sources*. [Online] *196(2011),* pp. 5357-5363. Available: https://www.sciencedirect.com/science/article/pii/S0378775310013534

[28] L. Lu et al. (2013, Mar.). A review on the key issues for lithium-ion battery management in electric vehicles. *Journal of Power Sources*. [Online] *226(2013),* pp. 272-288. Available: https://www.sciencedirect.com/science/article/pii/S0378775312016163.

[29] K.S. Ng, C-S. M, Y-P. Chen, Y-C. Hsieh, “Enhanced coulomb counting method for estimating state-of-charge and state-of-health of lithium-ion batteries,” Dept. of Electrical Engineering, National Sun Yat-sen University, Kaohsiung City, Taiwan, Jan. 8, 2009.

[30] C. Lin, X. Zhang, R. Xiong, F. Zhou, “A Novel Approach to State of Charge Estimation using Extended Kalman Filtering for Lithium-ion Batteries in Electric Vehicles,” in Transportation Electrification Asia-Pacific, Beijing, China, 2014, pp. 1.

[31] M. Cole, C. K. Lee, C. Zhu, W. G. Hurley, “State-of-Charge Determination From EMF Voltage Estimation; Using Impedance, Terminal Voltage, and Current for Lead-Acid and Lithium-Ion Batteries,” IEEE Trans. Ind. Electron., vol. 54, no. 5, pp. 1-8, Oct. 2007.

[32] Y. Xing, W. He, M. Pecht, K. L. Tsui, “State of charge estimation of lithium-ion batteries using open-circuit voltage at various ambient temperatures,” Department of systems Engineering and Engineering Management, City Univ. of Hong Kong, Hong Kong, China, Aug. 7, 2013.

[33] N. Watrin, B. Blunier, A. Miraoui, “Review of adaptive systems for lithium batteries State-of-Charge and State-of-Health estimation,” in Transportation Electrification Conf. and Expo., Dearborn, MI, 2012, pp. 1-6.

[34] Y. Zou, X. Hu, H. Ma, S.E. Li, “Combined State of Charge and State of Health estimation over lithium-ion battery cell cycle lifespan for electric vehicles,” National Engineering Lab for Electric Vehicles, Beijing Institute of Technology, Beijing, China, Oct. 2014.

[35] J. Kim, B.H. Cho, "State-of-Charge Estimation and State-of-Health Prediction of a Li-Ion Degraded Battery Based on an EKF Combined With a Per-Unit System," IEEE Trans. Veh. Technol., vol. 60, no. 9, pp. 1-12, Nov. 2011.

[36] H. He, R. Xiong, X. Zhang, F. Sun, J.X. Fan, "State-of-Charge Estimation of the Lithium-Ion Battery Using an Adaptive Extended Kalman Filter Based on an Improved Thevenin Model," IEEE Trans. Veh. Technol., vol. 60, no. 4, pp. 1-9, May 2011.

[37] Z. Yu, R. Huai, L. Xiao, "State-of-Charge Estimation for Lithium-Ion Batteries Using a Kalman Filter Based on Local Linearization," College of Mechanical and Electrical Engineering, Shandong University of Science and Technology, Qingdao, China, July 30, 2015.

[38] J. E. Bester, A. E. Hajjaji, and A. M. Mabwe, "Modelling of Lithium-ion Battery and SOC Estimation using Simple and Extended Discrete Kalman Filters for Aircraft Energy Management," presented at the IEEE Industrial Electronics Society, Yokohama, Japan, Nov. 9-12, 2015.

[39] S. Lee, J. Kim, J. Lee, B.H. Cho, "State-of-charge and capacity estimation of lithium-ion battery using a new open-circuit voltage versus state-of-charge," School of Electrical engineering and Computer Science, Seoul National University, Seoul, Korea, Sept. 21, 2008.

[40] F. Sun et al. (2011, May). Adaptive unscented Kalman filtering for state of charge estimation of a lithium-ion battery for electric vehicles. *Energy*. [Online]. *36(5)*, pp. 3531-3540. Available: https://www.sciencedirect.com/science/article/pii/S0360544211002271

[41] C. Speltino, A. Stefanopoulou, and G. Fiengo, "Cell equalization in battery stacks through State Of Charge estimation polling," presented at the American Control Conf., Baltimore, MD, June 30 – July 2, 2010.

[42] A. Salkind, C. Fennie, P. Singh, T. Atwater, D.E. Reisner, "Determination of state-of-charge and state-of-health of batteries by fuzzy logic methodology," UMDNJ-Robert Wood Johnson Medical School, Piscataway, NJ, Jan. 1999.

[43] X. Hu, F. Sun, Y. Zou, "Estimation of State of Charge of a Lithium-Ion Battery Pack for Electric Vehicles Using an Adaptive Luenberger Observer," School of Mechanical Engineering, Beijing Institute of Technology, Beijing, China, Sept. 2010.

[44] J. Xu, C.C. Mi, B. Cao, J. Deng, Z. Chen, S. Li, "The State of Charge Estimation of Lithium-Ion Batteries Based on a Proportional-Integral Observer," IEEE Trans. Veh. Technol., vol. 63, no. 4, pp. 1-8, May, 2014.

[45] T. Hansen and C. J. Wang. (2005, Mar.). Support vector based battery state of charge estimator. *Journal of Power Sources*. [Online]. *141(2)*, pp. 351-358. Available: https://www.sciencedirect.com/science/article/pii/S0378775304010626

[46] Xuezhe Wei and Bing Zhu (2009) The Research of Vehicle Power Li-ion Battery Pack Balancing Method. Paper presented at Conf. on Electronic Measurement & Instruments (ICEMI), Beijing, China, 16-19 Aug. 2009

[47] V. L. Teofilo, L. V. Merritt and R. P. Hollandsworth (1997) Advanced lithium ion battery charger. Paper presented at IEEE Battery Conf. on Applications and Advances, Long Beach, CA, 14-17 Jan. 1997

[48] Kong Zhi-Guo, Zhu Chun-Bo, Lu Ren-Gui, Cheng Shu-Kang (2006) Comparison and evaluation of charge equalization technique for series connected batteries. Paper presented at 37th IEEE Power Electronics Specialists Conference (PESC), Jeju, South Korea, 18-22 June 2006

[49] Sathish Kumar Kollimalla and Mahesh K. Mishra (2012) Analysis and Control of Buck-Boost Converter Using Average Power Balance Control (APBC). Paper presented at 2012 IEEE India Conference (INDICON), Kochi, India, 7-9 Dec. 2012

[50] Yuang-Shung Lee, and Ming-Wang Cheng (2005) Intelligent control battery equalization for series connected lithium-ion battery strings. IEEE Transactions on Industrial Electronics 52(5):1297-1307.doi: 10.1109/TIE.2005.855673

[51] Jian Cao, Nigel Schofield and Ali Emadi (2008) Battery Balancing Methods: A Comprehensive Review. Paper presented at the 2008 IEEE Vehicle Power and Propulsion Conference (VPPC), Harbin, China, 3-5 Sept. 2008

[52] Masatoshi Uno and Koji Tanaka (2011) Influence of High-Frequency Charge–Discharge Cycling Induced by Cell Voltage Equalizers on the Life Performance of Lithium-Ion Cells. IEEE Trans. on Vehicular Technology 60(4):1505-1515.doi: 10.1109/TVT.2011.2127500

[53] J. Shim et al. (2002, Oct.). Electrochemical analysis for cycle performance and capacity fading of a lithium-ion battery cycled at elevated temperature. *Journal of Power Sources*. [Online]. *112(1)*, pp. 222-230. Available: https://www.sciencedirect.com/science/article/pii/S0378775302003634

[54] A. Barre et al. (2013, Nov.). A review on lithium-ion battery ageing mechanisms and estimations for automotive applications. *Journal of Power Sources*. [Online]. *241(1)*, pp. 680-689. Available: https://www.sciencedirect.com/science/article/pii/S0378775313008185

[55] G. Nang and B. N. Popov. (2004, Sept.). Cycle Life Modeling of Lithium-Ion Batteries. *Journal of the Electrochemical Society*. [Online]. *151(10)*, pp. 1584-1591. Available: http://jes.ecsdl.org/content/151/10/A1584.short

[56] B. Xu et al. (2016) Modeling of Lithium-Ion Battery Degradation for Cell Life Assessment. IEEE Trans. On Smart Grid 9(2):1131-1140.doi: 10.1109/TSG.2016.2578950

[57] Y. S. Lee et al., “Battery Equalization Using Bi-directional Cûk Converters in DCVM Operation,” presented at IEEE Power Electronics Specialists Conf., Recife, Brazil, June 16, 2005.

[58] L. Yuang-Shung and D. Yiun-Yi. (2005, Oct.). Fuzzy-controlled individual-cell equaliser using discontinuous inductor current-mode Cuk convertor for lithium–ion chemistries. *IEE Proceedings - Electric Power Applications*. [Online]. *152(5),* pp. 1271-1282. Available: https://ieeexplore-ieee-org.uproxy.library.dc-uoit.ca/document/1516817/

[59] X. Lu, W. Qian, and F. Z. Peng, “Modularized Buck-Boost + Cuk Converter for High Voltage Series Connected Battery Cells,” presented at IEEE Applied Power Electronics Conf. and Expo., Orlando, FL, Feb. 5-9, 2012.

[60] LG Chem, “Rechargeable Lithium Ion Battery Model: INR18650HG2 3000mAh,” INR18650HG2 datasheet, April 2014 [Revised Nov. 2014].

[61] D. W. Hart, “DC-DC Converters,” in *Power Electronics*, 1st ed. New York: McGraw-Hill, 2011, pp. 226-230.

[62] Energus Power Solutions Ltd., “Tiny BMS150A/750A,” Tiny BMS Datasheet, May 2016 [Revised August 2017].

[63] Panasonic, “Lithium Ion NCR18650,” NCR18650 Datasheet, 2012.